APPLICATIONS OF THE BOUNDARY ELEMENT METHOD FOR STRUCTURAL SHAPE OPTIMIZATION

A Dissertation

Presented to

the Faculty of the Graduate School

University of Missouri-Columbia

In Partial Fulfillment

of the Requirements for the Degree

Doctor of Philosophy

---

by

SHYUE-JIAN WU

Dr. ERIC SANDGREN Dissertation Supervisor

May, 1986

The undersigned, appointed by the Dean of the Graduate Faculty, have examined a dissertation entitled

Applications of the Boundary Element Method
for Structural Shape Optimization

Presented by Shyue-Jian Wu

a candidate for the degree of Doctor of Philosophy
and hereby certify that in their opinion it is worthy of acceptance.

[redacted]
Dr. Eric Sandgren, Supervisor

[redacted]
Dr. Roger C. Duffield

[redacted]
Dr. Donald L. Creighton

[redacted]
Dr. John P. Barton

[redacted]
Dr. Harold J. Salane

APPLICATIONS OF THE BOUNDARY ELEMENT METHOD FOR STRUCTURAL SHAPE OPTIMIZATION

Shyue-Jian Wu

Dr. Eric Sandgren Dissertation supervisor

ABSTRACT

In this study, applications of the boundary element method for two- and three-dimensional structural shape optimization are presented. The displacements and stresses of the structure are computed using the boundary element method and substructuring analysis. The boundary element method provides the capability and advantages of modeling the varied shape of the boundaries during the optimization process. The substructuring analysis of the boundary element method produces better accuracy of the solution and reduces the computer time. The corresponding nonlinear programming problem for the optimization is solved by the generalized reduced gradient method (OPT program, Gabriele, Ragsdell, 1976). The Bezier and B-spline curves or surfaces are introduced to describe the shape of the design. The control points on these curves or surfaces are considered as

design variables. The number of design variables is smaller than the number of the nodal points of the boundary element mesh. The optimal design objective is to minimize weight or peak stress of the structural element and to determine an optimum shape for the structure, subject to geometrical and stress constraints. The optimization method has been successfully applied to the structural shape optimization of plain stress, plain strain and three-dimensional elasticity problems.

DEDICATION

To my parents

ACKNOWLEDGEMENT

This dissertation was accomplished through the efforts of many individuals. First, I would like to acknowledge my supervisor, Dr. Eric Sandgren for his precise advice, sensible suggestions and constant assistance in my graduate study and research.

I am also grateful to my other committee members. Dr. Roger C. Duffield offers his assistance and experience with the Finite Element Method. Dr. Harold J. Salane shared his advice concerning Structural Mechanics. And I truly appreciate Dr.Donald L. Creighton and Dr. John P. Barton for their encouraging comments.

Finally, I would like to express my special thanks to my wife for her highly understanding and permanent support.

TABLE OF CONTENTS

LIST OF FIGURES

LIST OF TABLES

CHAPTER 1

INTRODUCTION

Structural design optimization has generally been reduced to the weight minimization of frame or shell structures where the optimization is limited to resizing of structural members to obtain optimum cross sections or thicknesses. Shape optimization deals with continuous structural components where the optimum shapes of the boundaries and the surfaces of the bodies are determined. During the past fifteen years, the finite element method has been extensively used in structural optimization, including successful application to shape optimization. In contrast, the boundary element method has only recently been considered for shape optimization.

Application of the finite element method for shape optimal design of structural components has some disadvantages. One major difficulty is that shape changes during the optimization process may require the refinement of the finite element mesh because the initial configuration of the finite element mesh may result in very distorted elements for the new shape. Also accurate evaluations of stresses on the boundary are important for some problems which are subject to stress constraints on the boundary.

With the finite element method, it is difficult to obtain accurate information on the boundary. These difficulties with the finite element method can be overcome by using the boundary element method to discretize the structure. The solutions obtained through the use of the boundary element method for elasticity problems at the boundary are more accurate than the corresponding results using the finite element method. All the degrees of freedom are at the boundary in the boundary element model. There is no need for internal cells, so that the element mesh is updated easily during the optimization process.

In this dissertation, applications of the boundary element method for two- and three-dimensional structural shape optimization are presented. The displacements and stresses of the structure are computed using the boundary element method and substructuring analysis. The boundary element method provides the capability and advantages of modeling the varied shape of the boundary during the optimization process. The substructuring analysis of the boundary element method produces better accuracy and reduces the computer time. The corresponding nonlinear programming problem of the optimization is solved by the generalized reduced gradient method (OPT program, Gabriele, Ragsdell, 1976). Bezier and B-spline curves or surfaces are introduced to describe the shape of the design. The control points on these curves or surfaces are considered as design variables. The number of design variables is smaller than

the number of the nodal points of the boundary element mesh. The optimal design objective is to minimize weight or peak stress of the structural element and obtain an optimum shape for the structure, subject to geometrical and stress constraints.

To be specific, the purpose of this dissertation is as follows:

1. To develop a boundary element program for the analysis of two- and three-dimensional elasticity problems. The programs will have the capability to calculate the stresses and the displacements at any point in the structure.
2. To formulate the equations and develop a program for substructuring analysis by the boundary element method.
3. To apply the boundary element method for structural shape optimization.

Chapter 2 reviews the literature concerning structural shape optimization. Chapter 3 explains the development of the two- and three-dimensional boundary element programs. The basic formulae and numerical integration are introduced in chapter 3 as well as some numerical results for several elasticity problems which were generated and compared with finite element solutions. Chapter 4 introduces the capability of substructuring analysis by the boundary element method. A program which implements substructuring analysis has been developed. The numerical examples for the

substructuring analysis by the boundary element method are compared with the whole analysis of the boundary element method and the finite element method. Chapter 5 proposes the combination of the boundary element method and optimization. The model is applied to the shape optimal design of several elastic structural components. Chapter 6 presents conclusions of the study.

CHAPTER 2

LITERATURE SURVEY

The literature regarding optimal structural design is quite extensive (Ovadia 1981), but only a limited amount deals with the area of shape optimization. One of the first treatments of the general problem of the selection of the shape of a structure as part of the design objective is presented by Zienkiewicz and Cambell (1973). They formulate the shape optimal design problem using a finite element model of complex structures and treat the location of the nodal points of the finite element model as design variables. Then they calculate derivatives of stiffness and load matrices with respect to design variables and obtain derivatives of structural response measures and employ sequential linear programing to generate a numerical solution. They present examples associated with dams and rotating turbine machinery.

Kristensen and Madsen (1976) formulate a class of shape optimal designs for planar problems, which generalize the approach presented by Tvergaard (1975). They use orthogonal polynomials to locate the boundary of the body and treat the coefficients in these polynomials as design variables. They employ a finite element model of the structural response to

obtain derivatives of stress with respect to their design parameters and employ sequential linear programing to solve the optimization problem. They solve an elementary problem of the optimum shape of a hole in a biaxial stress field analytically and numerically illustrate the method on more complex problems. A generalized steepest decent method of optimal design for the shape optimization of two dimensional elastic bodies has been presented by Chun and Haug (1978). The design objective in this work is weight minimization, with constraints on Von Mises yield stress and shear stress distribution on the boundary. Schnack, (1979) used a finite element formulation for stress calculation in the neighborhood of a stress concentration and iteratively modified the contour to minimize peak stress.

Optimality criteria have been developed for selected classes of shape-optimal design problems, which have been used for constructing solutions. Kunar and Chan (1976) use a fully stressed design criteria and select geometrical variables to minimize weight. Dems and Mroz (1978) present a quite general approach to the shape-optimal design of an unloaded boundary of a structure. A boundary perturbation analysis is used to derive optimality criteria and a finite element method is used to determine optimum boundaries. Conditions for the global minimum of the mean compliance are generated.

Imam (1982) describes shape optimization of three dimensional structural components using the finite element

method. The objective function, mass ,is minimized by the direct use of the feasible direction method. The isoparametric representation of the surfaces and the numerical superposition of shape are discussed.

Braibant and Fleury (1984) have developed a model for shape-optimal design of two-dimensional elastic structures, based on isoparametric quadratic finite elements. Bezier curves and B-splines are introduced to describe the shape of the design. This technique reduces the number of design variables and avoids unrealistic designs. An analytical derivation of design sensitivity analysis with the finite element method used is presented. The objective function is to minimize the weight of the structure, with constraints on displacements and stresses. The model is applied to the design of several structural components.

The boundary element method has recently been applied to the shape-optimal design of solid and hollow shafts by Mota Soares, Rodriques, Oliveria Faria and Haug (1983) The design objective is to minimize torsional stiffness. The problem is formulated by the constant boundary element.

Mota Soares, Rodriques and Choi (1984) present the shape-optimal design of two-dimensional elastic components using the boundary element method. The design objective is to minimize the compliance of the structure, subject to an area constraint. The nodal variables of the boundary elements are taken as design variables. The boundary elements are composed of both linear and quadratic elements.

In the articles reviewed above, the finite element method was used for the structural analysis of most structural shape optimization methods. Structural shape optimization had only been applied to limited classes of problems. In this research, the boundary element method is used for the structural analysis of structural shape optimization. The optimization method described herein can be applied to the structural shape optimization of plain stress, plain strain and three-dimensional elasticity problems.

CHAPTER 3

DEVELOPMENT OF THE BOUNDARY ELEMENT PROGRAM

3.1 Introduction

One of the most popular numerical techniques which engineers and scientists everywhere are applying is the finite element method. This technique discretizes the domain of the problem under consideration into a number of elements. The governing differential equations of the problem are then approximated over the region by functions which fully or partially satisfy the boundary conditions. In addition, an alternative numerical technique has been developed in last few years. This technique is called the boundary integral method. The essence of the boundary integral method is the transformation of the differential equation into equivalent sets of integral equations. The transformation is from one over the domain to one over the boundary. It is sufficient for the solution of the problem to discretize only the boundary (hence the name, boundary element method), rather than the whole domain.

In recent years, the boundary element method has been increasingly used for solution of continuum mechanics problems. Applications include linear, non-linear,

steady-state and transient problems in solid and fluid mechanics. The importance of the boundary element method is that it reduces the dimensionality of the problem by one, which greatly simplifies the use of the computer program, and also generates much smaller systems of simultaneous equations for final solution.

The boundary element method involves modeling only the boundary geometry of the system. Once the necessary boundary information has been obtained, then the displacement and stress at any point in the domain or on the boundary can be calculated in terms of known boundary conditions.

3.2 Basic Equations of the Boundary Element Method

A complete mathematical development of the boundary element method has been given in a number of texts (Banerjee and Butterfield 1979, 1980; Brebbia 1978 ,1981, 1982, 1983; Jaswon and Symn 1978). The basic equations of the boundary element method for elasticity are based on Somigliana's integral equations. This equation for displacement in the absence of body forces is given by

$$C_{ij}(P)u_j(P)=\int_S \{t_i(Q)G_{ij}(P,Q)-u_i(Q)F_{ij}(P,Q)\}ds \qquad (3\text{-}1)$$

$u_j(P)$ is the displacement vector at a point P in the interior of the body or on the boundary, and $u_i(Q)$ and $t_i(Q)$

are the values of displacement and traction at the boundary point Q. $C_{ij}(P)$ is a coefficient that depends on the geometry of the boundary at point P. If point P is in the interior of the body, $C_{ij}(P)$ equals to δ_{ij}. The tensors G_{ij} and F_{ij} are the fundamental Kelvin solutions for displacements and tractions due to a unit concentrated force in an elastic infinite body. For an isotropic plane strain problem:

$$G_{ij}(x^p, x^q)=C_1\left(C_2\delta_{ij}\ln\frac{1}{r}+\frac{y_i y_j}{r^2}\right) \tag{3-2}$$

$$F_{ij}(x^p, x^q)=\frac{C_3}{r^2}\left[C_4(n_j y_i-n_i y_j)+\left(C_4\delta_{ij}+\frac{2y_i y_j}{r^2}\right)y_k n_k\right] \tag{3-3}$$

For a plane stress problem, Young's Modulus E and Poisson's ratio ν are replaced by $\nu'=\nu/(1+\nu)$ and $E'=E/(1-\nu'^2)$ respectively.

For the 3-D isotropic problem:

$$G_{ij}(x^p, x^q)=\frac{C_1}{2}\frac{1}{r}\left[C_2\delta_{ij}+\frac{y_i y_j}{r^2}\right] \tag{3-4}$$

$$F_{ij}(x^p, x^q)=\frac{C_3}{2}\frac{1}{r^2}\left[C_4\left(n_j\frac{y_i}{r}-n_i\frac{y_j}{r}\right)+\left(\frac{3y_i y_j}{r^2}+C_4\delta_{ij}\right)\frac{y_k n_k}{r}\right] \tag{3-5}$$

where

$$C_1=1/(8\pi\mu(1-\nu))$$

$$C_2=3-4\nu$$

$C_3=-1/(4\pi(1-\nu))$

$C_4=1-2\nu$

$\mu=E/2/(1+\nu)$

$y_i=x_i^q-x_i^p$

$y_j=x_j^q-x_j^p$

$r^2=y_i y_i$

n_j is outward normal

i,j=1,2 for 2-D problem

i,j=1,2,3 for 3-D problem

Having obtained the unknown values of displacements and tractions, together with the specified values of displacements and tractions, the interior values of stresses can be calculated by the following equation

$$\sigma_{ij}(x^p)=\int_S [D_{kij}(x^q,x^p)t_k(x^q)-S_{kij}(x^q,x^p)u_k(x^q)]ds(x^q) \qquad (3-6)$$

where

$$D_{kij}=\frac{1}{r^a}[(1-2\nu)\{\delta_{ki}\frac{y_j}{r}+\delta_{kj}\frac{y_i}{r}-\delta_{ij}\frac{y_k}{r}\}+b\frac{y_i y_j y_k}{r^3}]\frac{1}{4a\pi(1-\nu)} \qquad (3-7)$$

and

$$S_{kij}=\frac{2\mu}{r^b}[b\frac{y_m n_m}{r}\{(1-2\nu)\delta_{ij}\frac{y_j}{r}+\nu(\delta_{ik}\frac{y_i}{r}+\delta_{jk}\frac{y_k}{r})-c\frac{y_i y_j y_k}{r^3}\}$$

$$+b\nu(n_i\frac{y_j y_k}{r^2}+n_j\frac{y_i y_k}{r^2})+(1-2\nu)(bn_k\frac{y_i y_j}{r^2}+n_j\delta_{ik}+n_i\delta_{jk})$$

$$-(1-4\nu)n_k\delta_{ij}]\frac{1}{4a\pi(1-\nu)} \qquad (3-8)$$

The above formulae apply for two and three dimensional cases, i.e.

(1) a=1,b=2,c=3, i,j,k,m=1,2 for 2-D problem

(2) a=2,b=3,c=5, i,j,k,m=1,2,3 for 3-D problem.

3.3 Numerical Formulation of the Boundary Element Method

Except for a few simple problems, a closed-form solution for equation (3-1) is not available. Therefore a numerical method of solution has to be developed. The numerical solution of equation (3-1) is obtained by choosing a finite element approximation for the unknowns {u} and {t} on the boundary and employing a point collocation method for the integration. The boundaries may be represented by line elements in two-dimensional problems (Figure 3-1) and surface elements in three-dimensional problems (Figure 3-2), defined by their nodal coordinates. Within each element,the field variables such as geometry, displacement, and traction fields can be assumed to be constant, linear or quadratic depending upon the selection of the shape function. One has flexibility in discretizing the boundary and selecting the order of the expansion. The simplest boundary discretization is to employ straight elements. Curved elements allow more versatility in modeling complex shapes. In this dissertation, isoparametric linear and quadratic line elements (Figure 3-3) are selected for modeling the two-dimensional problem. The isoparametric linear and

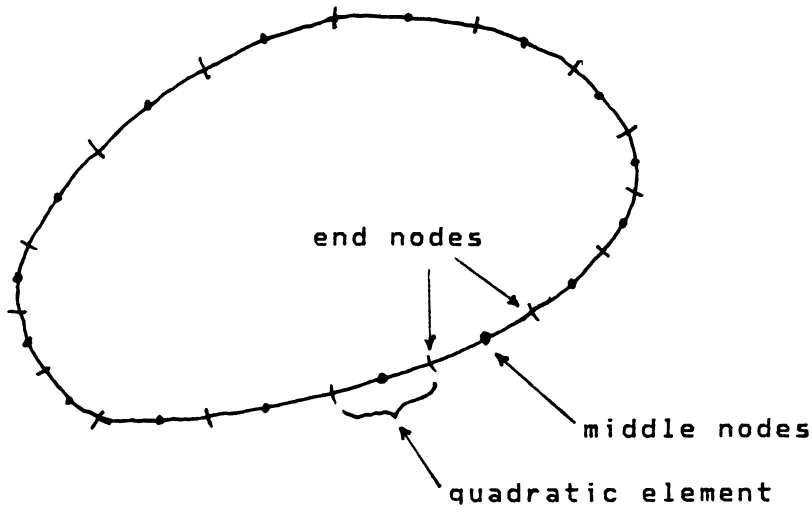

Figure 3-1 Boundary Element Mesh for a Two-dimensional Problem

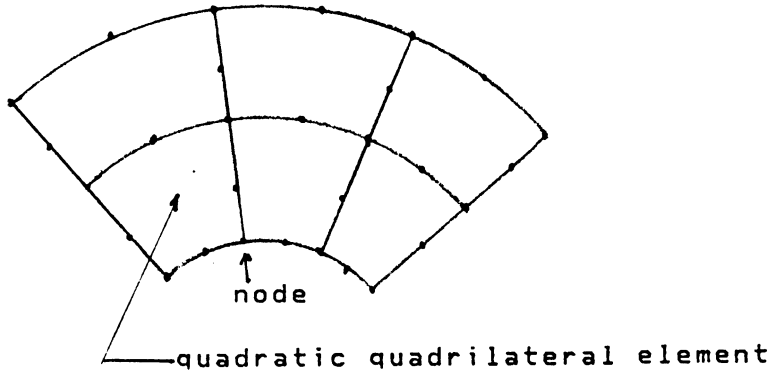

Figure 3-2 Boundary Element Mesh for one of the Surfaces of a Three-dimensional Problem

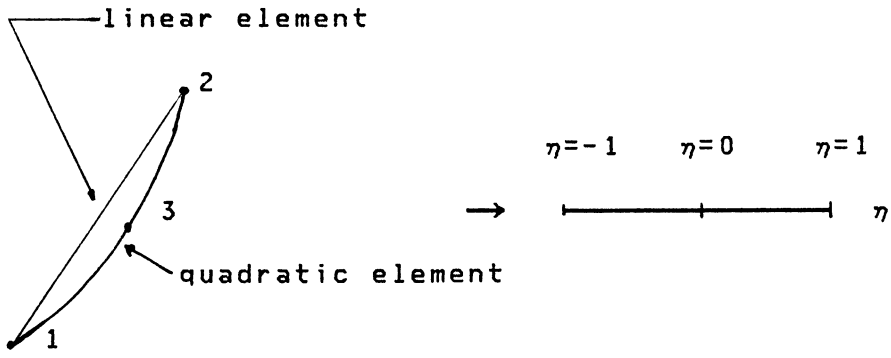

shape functions

(a) linear element

$N_1 = (1+\eta)/2$

$N_2 = (1-\eta)/2$

(b) quadratic element

$N_1 = \eta(\eta-1)/2$

$N_2 = \eta(\eta+1)/2$

$N_3 = 1-\eta^2$

Figure 3-3 Isoparametric Linear and Quadratic Line Elements and Their Shape Functions

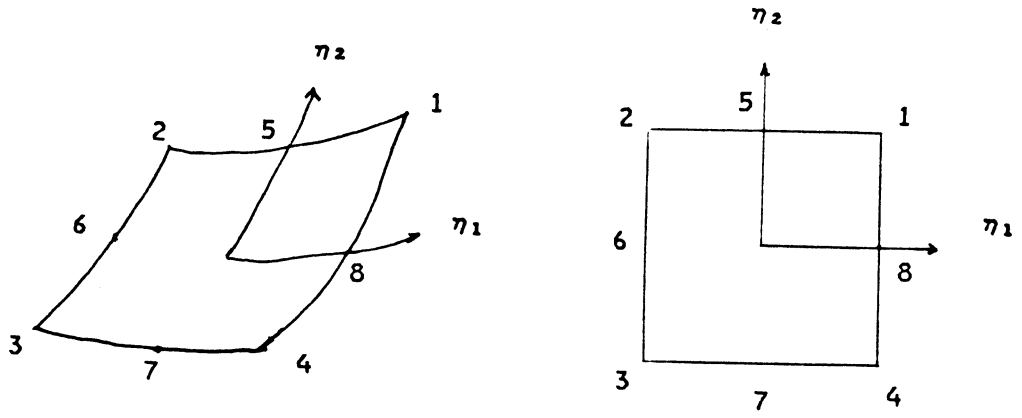

----- linear element

——— quadratic element

shape functions

(A) linear element

$N_1=(1+\eta_1)(1+\eta_2)/4$ $N_3=(1-\eta_1)(1-\eta_2)$

$N_2=(1-\eta_1)(1+\eta_2)/4$ $N_4=(1+\eta_1)(1-\eta_2)$

(b) quadratic element

$N_1=(1+\eta_1)(1+\eta_2)(\eta_1+\eta_2-1)/4$

$N_2=(1-\eta_1)(1+\eta_2)(-\eta_1+\eta_2-1)/4$

$N_3=(1-\eta_1)(1-\eta_2)(-\eta_1-\eta_2-1)/4$

$N_4=(1-\eta_1)(1+\eta_1)(1+\eta_2)/2$

$N_5=(1-\eta_1)(1+\eta_2)(1-\eta_2)/2$

$N_6=(1-\eta_1)(1+\eta_2)(1-\eta_2)/2$

$N_7=(1+\eta_1)(1-\eta_1)(1-\eta_2)/2$

$N_8=(1+\eta_1)(1-\eta_2)(1+\eta_2)/2$

Figure 3-4 Isoparametric Linear and Quadratic Quadrilateral Elements and Their Shape Functions

quadratic quadrilateral elements (figure 3-4) are used for solving the three-dimensional problem.

The value of the field variable over each element is in terms of nodal values and shape functions, the same as for finite element methods. Thus the field variable over the element is expressed in the form

$$\Phi(\eta)=N^{a}(\eta)\Phi^{a} \qquad a=1,2,....n \qquad (3-9)$$

where

N^{a} are shape functions of local coordinate η, $(-1\leq\eta\leq 1)$. The shape functions of line and surface elements are shown in Figures 3-3 and 3-4.

Φ^{a} are the values of the field variables at nodal points.

n is the total number of nodes on every boundary element. For example u in the x-direction over an isoparametric quadratic line element is given by $u_1= N^1 u_1{}^1+N^2 u_1{}^2+N^3 u_1{}^3$, where $u_1{}^1$, $u_1{}^2$, $u_1{}^3$ are nodal displacements at nodes 1,2,3 respectively. N^1, N^2, N^3 are shape fuctions of the isoparametric quadratic line elements (Figure 3-3).

If nodal coordinate, traction and displacement are introduced as field variables in Equation (3-9), then Equation (3-1) becomes a discetized form as

$$C_{ij}(x^{p})u_j(x^{p})=\sum_{k=1}^{M}\sum_{a=1}^{n}\{\int_{\Delta s_k}\{G_{ij}[x^{p},x^{q}(\eta_m)]N^{a}(\eta_m)J(\eta_m)ds(\eta_m)\}t_i{}^{a}-\int_{\Delta s_k}\{F_{ij}[x^{p},x^{q}(\eta_m)]n^{a}(\eta_m)J(\eta_m)ds(\eta_m)\}u_i{}^{a}\} \qquad (3-10)$$

where

M is the total number of boundary elements and

u_j^a is the value of u_j at local node a

t_j^a is the value of t_j at local node a

$J(\eta)$ is the jacobian of the transfomation of coordinates.

η_m is the local coordinate m=1 for 2-D problem, m=1,2 for 3-D problem.

i,j=1,2 for 2-D problem,i,j=1,2,3, for 3-D problem.

G_{ij},F_{ij} from Equation (3-2),(3-3) for 2-D and 3-D cases respectively.

The integral equation (3-1) finally reduces to an algebraic equation (3-10) by discetizing the boundary of the problem and substituting the field variables with nodal value and shape function. Noting that x^p refers to one of the element nodes, then collocation for all nodes on the boundary in turn, allows Equation (3-6) to be expressed in matrix form as follows:

$$[C]\{U\}+[H']\{U\}=[G]\{T\} \qquad (3\text{-}11)$$

or

$$[H]\{U\}=[G]\{T\} \qquad (3\text{-}12)$$

Where [H]=[C]+[H'] is obtained from the left hand side and the second term of the right hand side of equation (3-10),[C] is a tridiagonal matrix(2-D problem), which does not need to be determined explicitly. The tridiagonal coefficients in the [H] matrix (including [C]) can be obtained by applying rigid body conditions. If we apply a rigid body displacement to the body, then this will generate

no traction on the boundary (that is T=0). Therefore we can write Equation (3-12) as

$$[H]\{U\}=\{0\} \tag{3-13}$$

In order to satisfy the above equation for any system of arbitrary rigid body displacements each coefficient of the 2x2 on diagonal blocks(2-D problem) must be numerically equal to the sum of the corresponding coefficients of all off diagonal blocks with a change in sign. The 2x2 diagonal blocks contain the terms involving [C] as well as strongly singular integrals. In Equation (3-12), [G] is from the first term of the right hand side, and {U},and {T} include all surface nodal displacements and nodal tractions.

Applying the known boundary conditions, Equation (3-12) is rearranged, so all prescribed values are on one side and the unknowns on the other side, leading to a set of linear algebraic equations in terms of unknown nodal values

$$[A]\{x\}=\{f\} \tag{3-14}$$

where {x} and {f} are the vectors of unknown and known quantities respectively.

Once the integral equations are solved, the displacements at interior points can be calculated by Equation (3-1) with $C_{ij}=\delta_{ij}$, and the stresses at interior points can be calculated by Equation (3-6). The stress at any point on the boundary can be calculated as follow:

At any point X on the boundary, 15 quantities are defined: six stress components σ_{ij} and nine derivatives

$u_{i,j}$ where i,j=1,2,3. These quantities are described by 15 equations:

$$\sigma_{ij}=2\mu\epsilon_{ij}+\frac{2\mu\nu}{1-2\nu}\delta_{ij}\epsilon_{kk} \tag{3-15}$$

$$t_i=\sigma_{ij}n_j \tag{3-16}$$

$$\frac{du_i}{d\eta_m}=u_{i,j}\frac{dX_j}{d\eta_m} \tag{3-17}$$

where η_m, m=1,2 are the local coordinates of the boundary, and t_i i=1,2,3 and $(du_i/d\eta_m)$ are known quantities on the boundary. The values $(du_i/d\eta_m)$ can be calculated by finite differences or by directly differentiating the function u_i.

The 15 equations lead to a regular linear system for the unknown quantities σ_{ij} and u_{ij}. In plane 2-D problems the number of unknowns is reduced from 15 to 7, then i,j=1,2 and m=1.

3.4 Numerical Treatment of Integral Equations

The integrals appearing in Equation (3-10) are evaluated using ordinary Gaussian quadrature formulae:

$$\int_{-1}^{1} f(\xi)d\xi=\sum_{i=1}^{m} A_i f(\xi_i) \tag{3-18}$$

and

$$\int_{-1}^{1}\int_{-1}^{1} f(\xi_1,\xi_2)d\xi_1 d\xi_2=\sum_{i=1}^{m_1}\sum_{j=1}^{m_2} A_i A_j f(\xi_i,\xi_j) \tag{3-19}$$

for the line and surface area integrals respectively, where

f=(G,F)NJ,

A_i, A_j weight coefficients, and

ξ_i, ξ_j are the coordinates of integration points,

G,F are the kernel functions in Equation (3-2) to Equation (3-5) and

N is a shape function.

Unfortunately, in contrast to the integrals arising in the finite element method for elasticity problems, some of the integrals in the boundary element method are singular. If a collocation point belongs to the element on which it is located, Equation (3-10) has a singularity in its' integral form. These singular functions play a major role in all boundary element methods. The success of a boundary element program will greatly depend on the efficiency with which the calculation of the matrix elements in Equation (3-10) is performed and thus it is a crucial item in the whole process.

There are two different cases:

(i). $x^P \notin \Delta S_k$ and (ii) $x^P \in \Delta S_k$

Case (i) is a more straightforward case. We can use ordinary Gaussian quadrature formulae such as Equation (3-19), but the order of numerical integration to be used in the evaluation of the various boundary element integrals needs to be determined. The choice of the order of numerical integration is important, because the cost of analysis increases when a higher-order integration is

employed. Using a lower-order integration , the results can be affected by a very large amount. In general, the order (2m-1) is integrated exactly for the complete polynomial of degree m. But an invariant integration formulae is wasteful of computational time especially in the case of the three-dimensional formulation. The order of integration can be varied by determining the distance from the field point to the element and the size of element. Therefore it is necessary to incorporate in the algorithm an automatic choice of the orders of Gaussian quadrature formulae (the parameters m, m_1, m_2) and to preserve the convergence of integration. This has been accomplished by Lachat and Watson 1976

In case (ii), the integral requires special treatment due to singularities of the integrands. For 2-D problems the integral involving G_{ij} is of the type

$$\int_{-1}^{1} \ln(1/r) f(\xi) d\xi \qquad (3\text{-}20)$$

If the singularity is on an end node of a linear or quadratic element (Figure 3-5a), this integral can be transformed to

$$\int_{-1}^{1} \ln\frac{1}{r} f(\xi) d\xi = \int_{-1}^{1} \ln\left(\frac{1+\xi}{2r}\right) f(\xi) d\xi + 2\int_{0}^{1} \ln\frac{1}{\beta} f(\beta) d\beta \qquad (3\text{-}21)$$

where $\beta = (1+\xi)/2$.

If the singularity is on a middle node of a quadratic element (Figure 3-5b), Equation (3-20) becomes

$$\int_{-1}^{1} \ln\frac{1}{r} f(\xi)d\xi = \int_{-1}^{1} \ln\frac{|\xi|}{r} f(\xi)d\xi + \int_{0}^{1} \ln\frac{1}{|\xi|} f(\xi)d\xi,$$

$$+ \int_{0}^{1} \ln\frac{1}{|\xi|} f(-\xi)d\xi, \qquad (3\text{-}22)$$

The integrand in the first integral of Equation(3-21) or (3-22) can be easily shown to be bounded and therefore we use the ordinary Gaussian quadrature while the second and third integrals are evaluated numerically by formulas given by Stroud and Secrest(1966);

$$\int_{0}^{1} \ln\frac{1}{\xi} f(\xi)d\xi = \sum_{i=1}^{m} B_i f(\xi_i) \qquad (3\text{-}23)$$

where B_i are weight coefficients and ξ_i are coordinates of integration points.

For 3-D problems the integrals corresponding to Equation(3-10) present a 1/r singularity of the following type

$$\int_{-1}^{1}\int_{-1}^{1} \frac{1}{r} f(\xi_1, \xi_2)d\xi_1 d\xi_2 \qquad (3\text{-}24)$$

For the quadrilateral element, the element is subdivided into triangular subelements, according to the location of the point x^p (Figure 3-6)

The subelement can be transformed to a local polar coordinate system (ρ, θ), with origin at x^p where the element

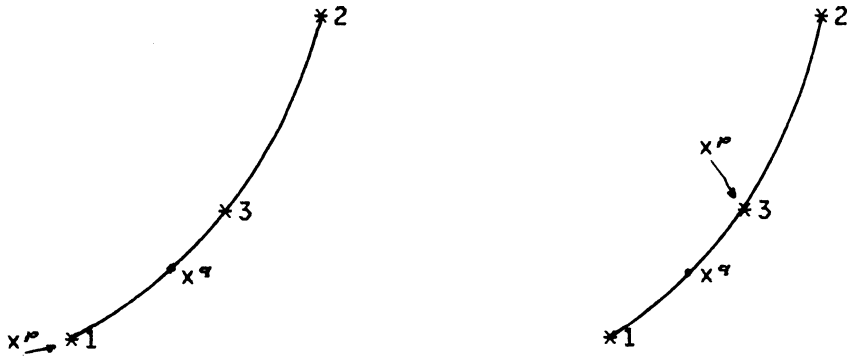

Figure 3-5 Field Point x^p is in a Line Element Itself

(a)X^p at End Node of the Element

(b)x^p at Middle Node of the Element

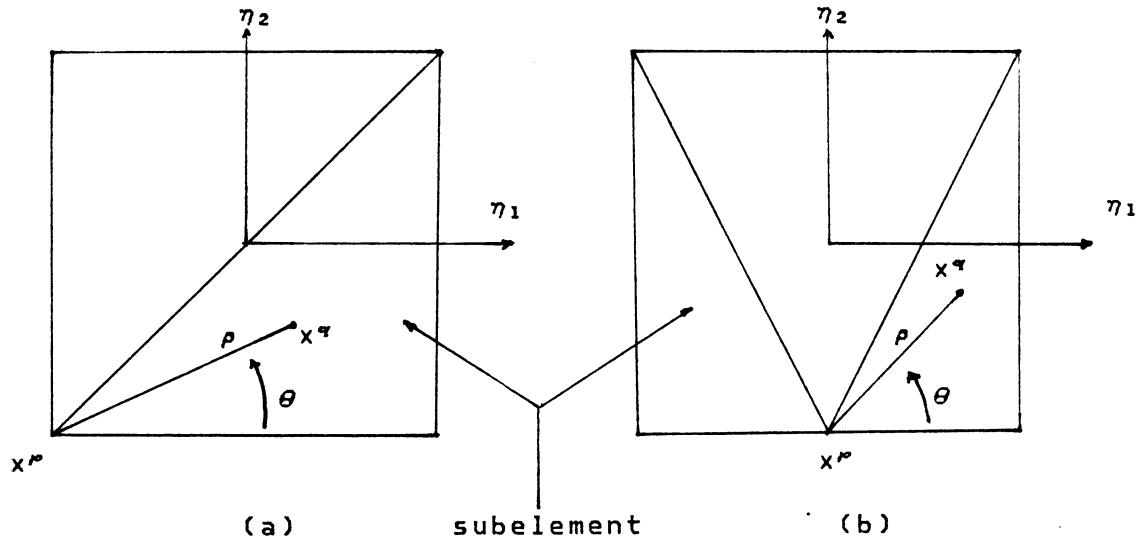

Figure 3-6 Field point x^p is in a quadrilateral element itself. (a) x^p at corner node of element. (b) x^p at mid-side node of element.

area $d\xi_1 d\xi_2$ becomes $\rho d\rho d\theta$. Therefore the integral over the element is made up of integrals over each subelement. The integral Equation (3-24) becomes

$$\sum_{i=1} \int_{\Delta_i} \frac{1}{r} f(\rho,\theta)\rho d\rho d\theta \qquad (3\text{-}25)$$

where Δ_i represents a triangular subelement. The singularity of Equation (3-25) is reduced by cancellation of ρ and r. Then the remaining integral form can be calculated by ordinary Gaussian formulae.

3.5 Description of the Program

Based on the mathematical theory and numerical treatment introduced earlier, the boundary element method has been implemented in a computer program. The logical sequence of steps is:

(1) Generation of input data defining the geometry of the boundary elements.

(2) Integration of kernel shape function products to generate the system matrix.

(3) Solution of the system of equations to get the unknown boundary data

(4) Calculation of interior information by obtained boundary data.

A brief flow chart of the boundary element program is illustrated as Figure (3-7). The main program BEM calls subroutines GAUSS, INPUT, BEMAT, BSOLVE, BINSD, and BSD. Subroutine GAUSS forms the weights and integration points for the Gaussian formulae. Subroutine INPUT reads the data relating the geometry, boundary conditions, and material properties.

Subroutine BEMAT sets up the coordinates of the boundary nodes for point collocation and calls subroutine DINTEG to calculate the [G] and [H] matrices for each boundary collocation point. Subroutine DINTEG sets up the local axis system on the boundary elements, calculates the order of integration formulae, the jacobian, and integrates the kernel-shape function products to generate coefficients for the matrices [G] and [H] for a specified boundary or interior field point. Subroutine SINTEG generates the coefficient matrices [D] and [S] to calculate stresses in the domain.

Subroutine BSOLVE assembles the final system of equations for the specified boundary conditions. The values of the boundary tractions and displacements are also calculated. Subroutine BSD transforms the boundary tractions to boundary stresses and calculates displacements and stresses on any seleted boundary point. Subroutine BINSD calculates displacements and stresses at interior points.

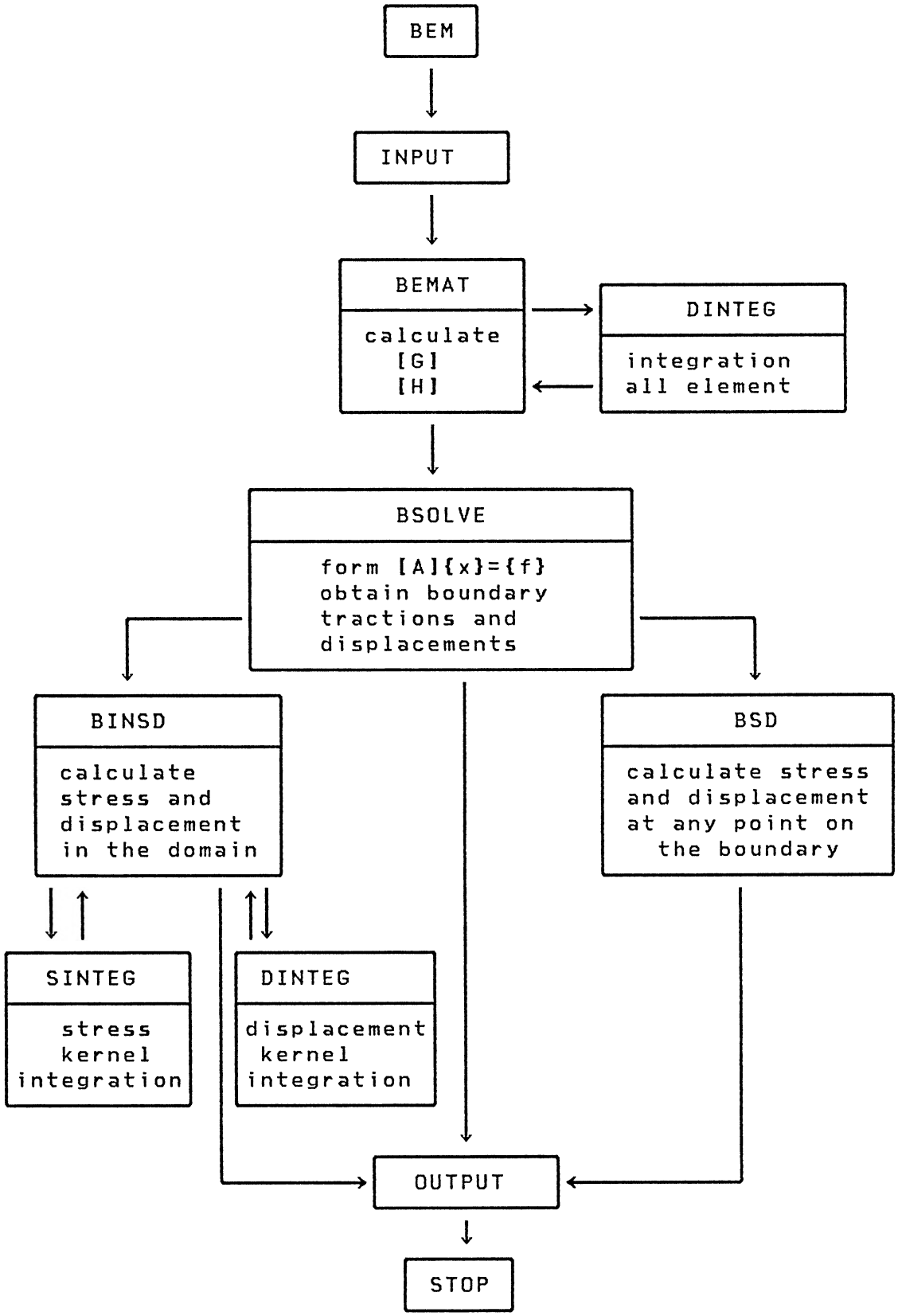

Figure 3-7 Brief Flow Chart of the Boundary Element Method

3.6 Numerical Results and Comparison to the Finite Element Solution

Several different examples have been chosen to test the BEM program. The results are also compared to the corresponding finite element model which is solved by GTSTRUDL (1983). All the following computations were performed on the same computer (VAX 11/780) which means that the results are comparable. The examples include:

(1) A thick wall cylinder under internal pressure

(2) Bending of a beam under uniform load

(3) A cylindrical cavity under internal pressure

(4) A three-dimensional rod subjected to a uniform axial tension

(5) Bending of a three-dimensional cantilever beam under end load

3.6.1 A Thick Wall Cylinder under Internal Pressure

The cross-sectional geometry and loading for the problem is illustrated in Figure (3-8). The material properties are taken as $E=1.0\times10^{6}$ lb/in^2 and $\nu=0.3$. Due to symmetry only one quarter of the structure has been modeled. This problem has been discretized using 12 isoparametric quadratic finite elements with 51 nodes. The isoparametric quadratic boundary elements with the same mesh on the boundary have 14 elements and 28 nodes. Figures (3-9) and

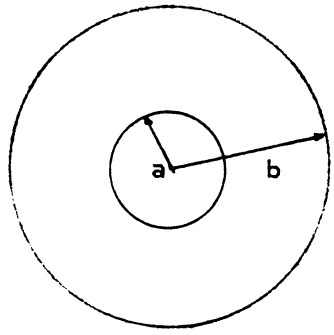

a=10 in
b=30 in
p=1000 psi(internal pressure)

Figure 3-8 Cross-section of Thick Wall Cylinder

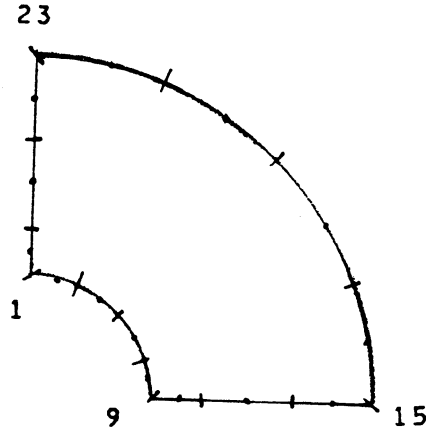

14 isoparametric
quadratic elements
28 nodes
54 d.o.f.

Figure 3-9 The Boundary Element Model for a Thick Wall Cylinder

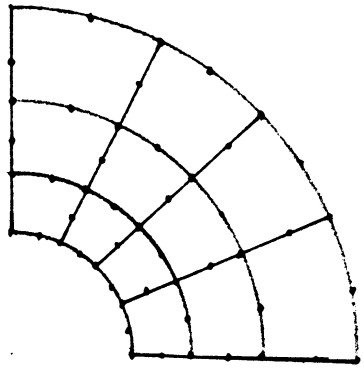

12 isoparametric
quadratic elements
51 nodes
102 d.o.f.

Figure 3-10 The Finite Elemet Model for a Thick Wall Cylinder

(3-10) represent the mesh used in the boundary element method and the finite element method. In Figure (3-9), all the elements are at the boundary of the boundary element model and there is no need for internal cells.

In Tables (3-1),(3-2),(3,3) a comparison of results is presented. The finite element analyses with refinements on the boundaries similar to those of the boundary element discretizations involve rather large numbers of nodes without obtaining better accuracy in the calculated stresses. However, more information is generally provided about the stress and displacement fields in the domain. The displacement finite element method gives good results for displacements but less accurate results for stresses, which are in most cases of greater interest to the engineer. Also note that the calculated stress field is discontinuous across element interfaces. In the boundary element analysis, the stress and displacement at any selected point can be calculated directly after the boundary tractions and displacements have been solved. In Table 3-1 and 3-2, the boundary element method shows better results for stresses.

3.6.2 Bending of a Beam under a Uniform Load

This example is a deep, simply supported beam subject to a uniformly distributed load. The geometry and loading for the problem are shown in Figure 3-11. The beam was

Table 3-1 Comparison of tangential stress for

Thick Wall Cylinder

radial distance (in)	exact[a] (psi)	FEM value (psi)	FEM error %	BEM value (psi)	BEM error %
10	1250.0	1270.71	1.66	1242.0	0.6
14	698.9	716.38	2.47	699.1	0.03
22	357.44	365.43	2.27	357.3	0.04
30	250.0	252.96	1.18	250.0	0.0

[a] Timoshenko and Goodier 1970

Table 3-2 Comparison of Radial Stress

for Thick Wall Cylinder

radial distance (in)	exact[a] (psi)	FEM value (psi)	FEM error %	BEM value (psi)	BEM error %
10	-1000.	-925.66	7.43	-1000.	0.
14	-448.98	-387.21	13.75	-448.7	0.06
22	-107.44	-79.51	26.59	-107.3	0.13
30	0.	10.44	--	0.	0.

[a] Timoshenko and Goodier 1970

Table 3-3 Comparison of Radial Displacement

for Thick Wall Cylinder

radial distance (in)	exact[a] ($x10^{-2}$ in)	FEM value ($x10^{-2}$ in)	FEM error %	BEM value ($x10^{-2}$ in)	BEM error %
10	1.55	1.549	0.07	1.549	0.07
14	1.167	1.167	0.00	1.166	0.09
22	.857	.857	0.00	.856	0.09
30	.75	.749	0.15	.749	0.15

[a] Timoshenko and Goodier 1970

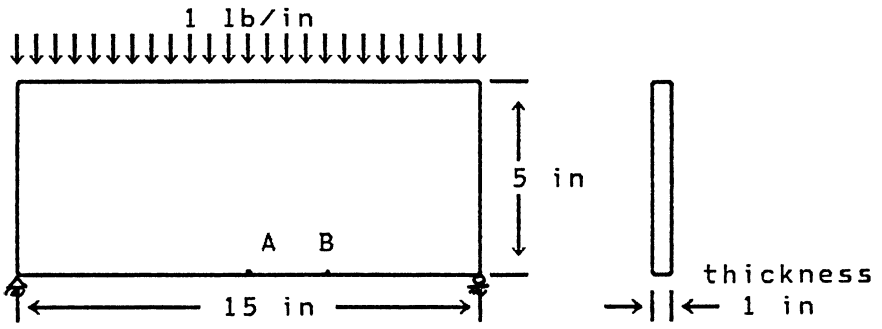

Figure 3-11 A Simply Supported Beam under Uniform Load

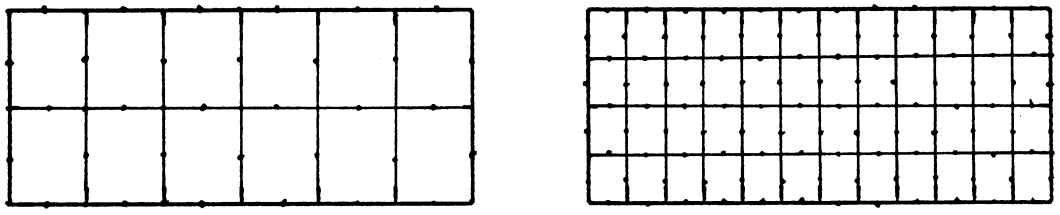

12 elements

48 elements

Figure 3-12 The Finite Element Mesh of a Beam

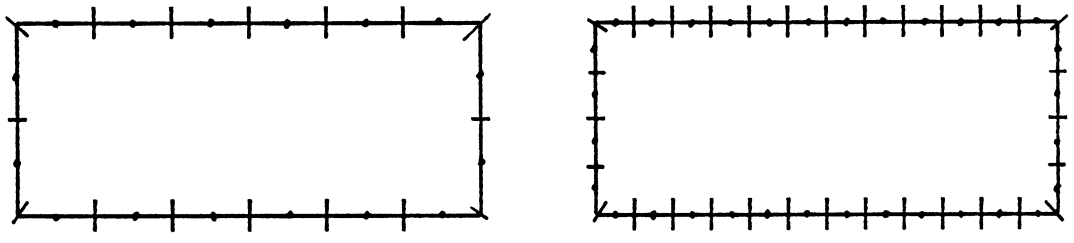

16 elements

32 elements

Figure 3-13 The Boundary Element Mesh of a Beam

analyzed as a plane stress case for different finite element and boundary element meshes.

For the finite element method the beam is represented by 12 eight-node isoparametric quadratic elements with 53 nodes and 48 refined meshes with 177 nodes (Figure 3-12). The boundary element models have the same boundary nodes as the finite element models. The boundary of the beam was divided into 16 isoparametric quadratic elements with 32 nodes and 32 refined meshes with 64 nodes (figure 3-13). The results are compared to an exact solution obtained from plane elasticity theory in Table 3-4.

From Figures 3-12 and 3-13, we can see the mesh refinement of the boundary element method is much easier than that for the finite element method. In Table 3-4, it is clear that as more elements are used the accuracy of both methods improves. The solution obtained using the 32-element BEM mesh and 48-element FEM mesh are in close agreement with the values given by the exact solution. The 32-element BEM mesh shows less data generation and computer time were required. Even the results obtained using a 12-element BEM are resonable and save significant computer time.

3.6.3 A Cylindrical Cavity under Internal Pressure

The following example shows the application of the boundary element method for the case of a cylindrical cavity

Table 3-4 Comparison of Deflection , Stress and Computer Time for a Simply Supported Beam under Uniform Load

method	logitudinal stress σ_{xx} (psi) at point A	vertical deflection u_y x10^{-6} (in) at point A	at point B	CPU time (sec)
exact solution[a]	6.95	.508	.462	---
BEM (16)	7.01	.503	.440	6.50
BEM (32)	6.957	.505	.443	32.43
FEM (12)	7.048	.496	.432	24.83
FEM (48)	6.966	.505	.442	98.30

[a] Timoshenko and Goodier 1970

under internal pressure in an infinite medium. The material properties are taken as $E=2.0\times10^5$ lb/in^2 and $\nu=0.1$. The boundary has been described by 48 linear and 24 quadratic elements (Figure 3.14)

In Table 3.5 and 3.6 exact results are compared to the boundary element solution and the agreement is satisfactory. The displacements and stresses decay with inceasing distance from the cavity. The radial stresses and tangential stresses at these internal points have the same absolute value but different sign which is correct. The solution generated using quadratic elements is better than the results with linear elements because the curved boundary is handled better by the higher order element.

3.6.4 A Three-dimensional Rod Subjected to a Uniform Axial Tension.

The geometry and loading for the problem are illustrated in Figure 3-15. The boundary of the beam was discretized by 10 isoparametric linear quadrilateral 4-node elements with 12 nodes and 36 degrees of freedom (Figure 3-16). Figure 3-17 shows a 20-node mesh of 6 isoparametric quadratic quadrilateral 8-node elements or 1 isoparametric quadratic 20-node hexahedron finite element. The results of the three analyses (Table 3-7) are close and accurate when compared to the exact solution.

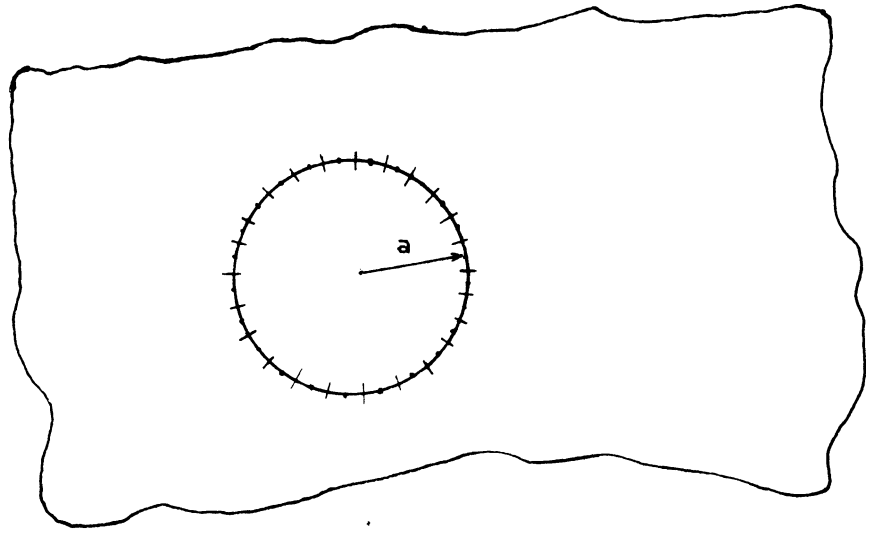

a=3 in
internal pressure=100 psi

Figure 3-14 A Cylindrical cavity under Internal Pressure in an Infinite Medium

Table 3-5 Comparison of Interior Displacement for Cylindrical Cavity under Internal Pressure in an Infinite Medium.

distance to the center of the cavity (in)	displacement (in)		
	exact[a]	BEM (lin.)	BEM (quad.)
3	1.650×10^{-3}	1.644×10^{-3}	1.650×10^{-3}
4	1.237×10^{-3}	1.231×10^{-3}	1.237×10^{-3}
10	4.950×10^{-4}	4.921×10^{-4}	4.950×10^{-4}
50	9.900×10^{-5}	9.841×10^{-5}	9.870×10^{-5}
100	4.950×10^{-5}	4.921×10^{-5}	4.935×10^{-5}
1000	4.950×10^{-6}	4.922×10^{-6}	4.920×10^{-6}

[a] Timoshenko and Goodier 1970

Table 3-6 Comparison of Interior Stress for Cylindrical Cavity under Internal Pressure in an Infinite Medium.

distance to the center of the cavity (in)	radial stress (lbs/in²)		
	exact[a]	BEM (lin.)	BEM (quad.)
3	-100.0000	-99.7900	-100.0000
4	-56.2500	-55.9500	-56.2500
10	-9.0000	-8.9500	-9.0000
50	-0.3600	-0.3581	-0.3600
100	-0.0900	-0.0895	-0.0900
1000	-0.0009	-0.000895	-0.0008998

[a] Timoshenko and Goodier 1970

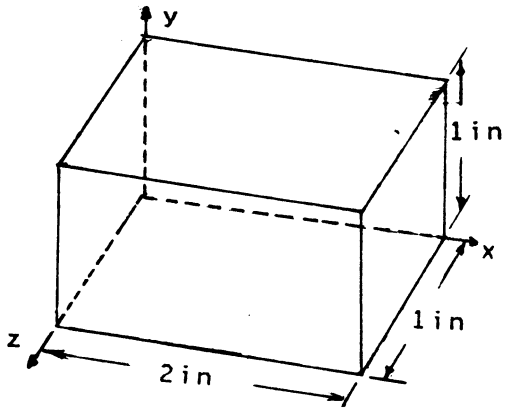

E=1.0 lb/in² ν= 0

boundary conditions:

t_x=1.0 at x=2.0

u_x= u_y= u_z=0 at x=0

t_x= t_y= t_z=0 at other nodes

Figure 3-15 A Rectangular Cross-sectional Rod

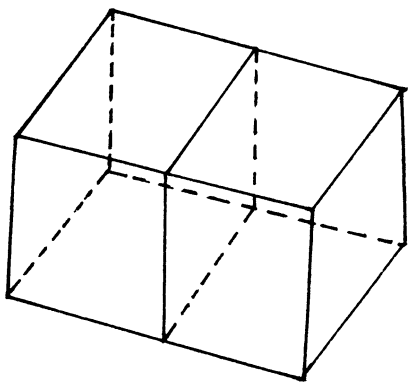

10 isoparametric linear quadralateral 4-node elements

12 nodes , 36 d.o.f.

Figure 3-16 The Linear Boundary Element Model for a Rectangular Cross-sectional Rod.

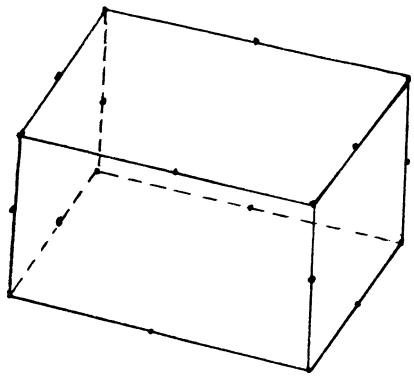

6 isoparametric quadratic quadralateral 8-node boundary elements
20 nodes , 60 d.o.f.
or 1 isoparametric quadratic 20-node hexahedron finite elements
20 nodes , 60 d.o.f.

Figure 3-17 The Quadratic Boundary and Finite element Model for a Rectangular Cross-sectional Rod.

Table 3-7 Comparison of Deflections and Stresses for a Ractangular cross-sectional Rod under Uniform Tension.

method	displacement u_x(in)		stress σ_{xx}(psi)	
	at x=1in	at x=2in	at x=0in	at x=1in
exact solution[a]	1.00000	2.0000	1.00000	1.0000
BEM (lin.)	0.99989	1.9997	0.99989	0.9998
BEM (quad.)	1.00000	2.0000	0.99998	0.9999
FEM (quad.)	.999999	1.9999	0.99999	1.0000

[a] Brebbia 1982

3.6.5 Bending of a Three-dimensional Cantilever Beam under End Load

The dimensions and loading for the problem are shown in Figure 3-18. Three analyses have been carried out using both linear and quadratic elements. The boundary has been divided into 32 isoparametric linear quadrilateral boundary elements (Figure 3-19) and 10 isoparametric quadratic quadrilateral boundary elements (Figure 3-20). The finite element model has the same number of nodes for 2 isoparametric quadratic 20-node hexahedron elements (Figure 3-20).

In Table 3-8, the results for the linear element have large errors, but the results for the quadratic element for both methods are close to the exact solution. The computational time of the BEM is larger than that of the FEM with the same number of nodes. The evaluation of each component of the matrices in a BEM solution involves more arithmetic calculation than does its finite element counterpart, thus will offset some of the computer time saved by the reduction of system matrices for bigger problems.

3.7 CONCLUSION

A boundary element program has been developed using linear and quadratic line and quadrilateral boundary

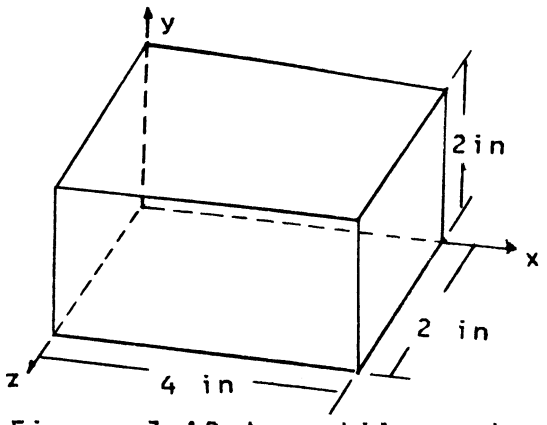

E=1.0 lb/in² ν= 0
boundary conditions:
t_y=-1.0 lb/in and
t_x=t_z=0 at x=2.0
u_x= u_y= u_z=0 at x=0
t_x= t_y= t_z=0 at other surfaces.

Figure 3-18 A cantilever beam

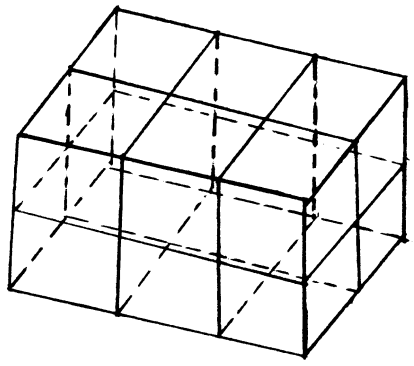

32 isoparametric linear quadralateral 4-node elements

34 nodes , 102 d.o.f.

Figure 3-19 The Linear Boundary Element Model for a Cantilever Beam

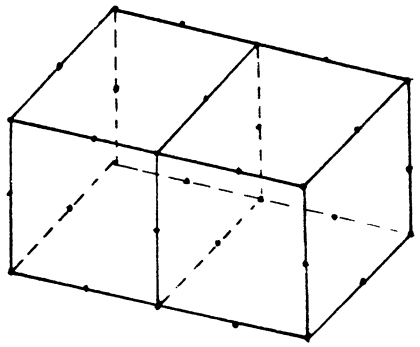

10 isoparametric quadratic quadralateral 8-node boundary elements

32 nodes , 96 d.o.f.

or 2 isoparametric quadratic 20-node hexahedron finite elements

20 nodes , 60 d.o.f.

Figure 3-20 The Quadratic Boundary and Finite Element Model for a Cantilever Beam

Table 3-8 Comparison of Deflections and stresses for a Cantilever Beam under End Load

method	deflection u_x (in) at x=4 in	stress σ_{xx} (psi) at y=2 in and x=0 in	x=2 in
exact solution[a]	-0.762×10^{-2}	12.0	6.0
BEM (lin.)	-0.581×10^{-2}	9.57	4.39
BEM (quad.)	-0.722×10^{-2}	11.78	6.11
FEM (quad.)	-0.716×10^{-2}	11.73	5.99

[a] Brebbia 1982

elements. Results for practical problems of two- and three-dimensional elasticity without body forces have been presented and the usage of different element types has been demonstrated. In general, the results show that the quadratic element is more efficient and accurate than the linear element. For problems with curved boundaries the quadratic element allows for a good representation of the curve outline.

If a boundary node is located at a corner, the tractions are specified by multiple values because of the discontinuity of the traction, but the displacements have unique values at each corner node. The stress at a node on a corner are the average values of the stresses at the same geometric point. The corner is defined so that the smaller angle of two connecting elements is less than 150 degrees. With this restriction the errors from boundary discontinuity are negligible. For example, the circular boundary of the problem in Section 3.6.1 was discretized by four quadratic elements to avoid the corners and the corner nodes 1,9,15,23 were defined by two traction nodes for each geometric point. The results shown in Tables 3-1, 3-2 are satisfactory.

As seen from the numerical results presented in the last section we can summarize the following advantages and disadvantages of the boundary element method when compared to the finite element method.

Advantages:

(1) Dimensionality of the problem is reduced.

(2) Less data is required to defined the problem and simple interpretation of results is possible.

(3) Accuracy is better with the same (even less) number of nodes.

(4) Transition from coarse to fine meshes is simplified.

(5) Ordering of nodes and elements is not important.

(6) Problem involving infinite domains are easy to solve.

Disadvantages:

(1) The system matrices are fully populated.

(2) The increased computational time required can not be offset by the reduced number of nodes when the ratio of surface to volume of the structure is large.

(3) If the problem requires a large number of internal points to be evaluated, the advantage of reduced computer time is lost.

(4) Material properties must be constant.

(5) Application for structural analysis has less versatility.

(6) Not knowing where peak stress is if it occurs in the interior.

CHAPTER 4

SUBSTRUCTURING ANALYSIS BY THE BOUNDARY ELEMENT METHOD

4.1 Introduction

The object of this chapter is to present the elastic analysis of structures using the substructuring concept with the boundary element method. The basic idea of substructuring analysis by the boundary element method comes from the substructuring analysis by the stiffness method (Przemieniecki,1963 and Rosen, Rubinstein,1970). The major difference between these two methods is the equilibrium equation of the structures, so the formulation of the final set of simultaneous equations is different. The substructuring analysis essentially consists of separate analyses of each substructure with all generalized displacements on common boundaries completely constrained. This is followed by the relaxation of these boundaries to ensure equilibrium and the calculation of the substructuring interfaced displacements.

In the substructuring concept, the final system equation is derived in terms of displacements of the interfaced nodes for the whole structure. Naturally, the system equation for the substructuring analysis involves a

considerably smaller number of unknowns compared with that for the complete structure without partitioning. The interfaced displacements are obtained first, then each substructure can be analyzed separately, again, under known interfaced displacements. This can be achieved without much difficulty since the substructures analyzed would be of relatively small size.

4.2 The Formulation of Substructuring Analysis

In the present substructuring analysis ,the total structure is partitioned into component substructures. For each substructure the coefficient matrices [G] and [H] are calculated separately by the boundary element method. The substructure is characterized by noninterfaced coordinates and interfaced coordinates where it is connected to adjacent substructures. The system of equations for a substructure may be written in a partitioned matrix form as

$$\begin{bmatrix} H_{ii} & H_{ib} \\ H_{bi} & H_{bb} \end{bmatrix} \begin{Bmatrix} u_i \\ u_b \end{Bmatrix} = \begin{bmatrix} G_{ii} & G_{ib} \\ G_{bi} & G_{bb} \end{bmatrix} \begin{Bmatrix} t_i \\ t_b \end{Bmatrix} \qquad (4\text{-}1)$$

where subscripts i and b denote noninterfaced coordinates and interfaced coordinates, respectively.

Equation (4-1) can be transformed into a new uncoupled system equation by the following decomposition transformation.

$$\begin{bmatrix} I & 0 \\ H_{bi}H_{ii}^{-1} & I \end{bmatrix}\begin{bmatrix} H_{ii} & 0 \\ 0 & H_{bb}{}^{b} \end{bmatrix}\begin{bmatrix} I & H_{ii}^{-1}H_{ib} \\ 0 & I \end{bmatrix}\begin{Bmatrix} u_i \\ u_b \end{Bmatrix}$$

$$= \begin{bmatrix} I & 0 \\ H_{bi}H_{ii}^{-1} & I \end{bmatrix}\begin{bmatrix} I & 0 \\ -H_{bi}H_{ii}^{-1} & I \end{bmatrix}\begin{bmatrix} G_{ii} & G_{ib} \\ G_{bi} & G_{bb} \end{bmatrix}\begin{Bmatrix} t_i \\ t_b \end{Bmatrix} \qquad (4\text{-}2)$$

The first matrix on both sides of the above equation can be cancelled. Then, Equation (4-2) can be written as an uncoupled system equation.

$$\begin{bmatrix} H_{ii} & 0 \\ 0 & H_{bb}{}^{b} \end{bmatrix}\begin{Bmatrix} U_i{}^{b} \\ U_b{}^{b} \end{Bmatrix} = \begin{Bmatrix} t_i{}^{b} \\ t_b{}^{b} \end{Bmatrix} \qquad (4\text{-}3)$$

where

$$H_{bb}{}^{b} = H_{ii} - H_{bi}H_{ii}^{-1}H_{ib} \qquad (4\text{-}4)$$

and

$$\begin{Bmatrix} u_i{}^{b} \\ u_b{}^{b} \end{Bmatrix} = \begin{bmatrix} I & H_{ii}^{-1}H_{ib} \\ 0 & I \end{bmatrix}\begin{Bmatrix} \\ u_b \end{Bmatrix} = \begin{Bmatrix} u_i + H_{ii}^{-1}H_{ib}u_b \\ u_b \end{Bmatrix} \qquad (4\text{-}5)$$

and

$$\begin{Bmatrix} \\ t_b{}^{b} \end{Bmatrix} = \begin{bmatrix} I \\ -H_{bi}H_{ii}^{-1} \end{bmatrix}\begin{bmatrix} \\ I \end{bmatrix}\begin{bmatrix} i \\ G \end{bmatrix}\begin{Bmatrix} \\ t_b \end{Bmatrix}$$

$$= \begin{Bmatrix} G_{ii}t_i + G_{ib}t_b \\ (G_{bi} - H_{bi}H_{ii}^{-1}G_{ii})t_i + (G_{bb} - H_{bi}H_{ii}^{-1}G_{ib})t_b \end{Bmatrix} \qquad (4\text{-}6)$$

The uncoupled system equation for each substructure related to the interface is

$$H_{bb}{}^{b}u_b{}^{b} = t_b{}^{b} \qquad (4\text{-}7)$$

i.e.

$$(H_{bb} - H_{bi}H_{ii}^{-1}H_{ib})u_b = (G_{bi} - H_{bi}H_{ii}^{-1}G_{ii})t_i + (G_{bb} - H_{bi}H_{ii}^{-1}G_{ib})t_b \qquad (4\text{-}8)$$

In order to separate the coefficients of the interfaced traction t_b, Equation (4-8) is premultiplied by $(G_{bb}-H_{bi}H_{ii}^{-1}G_{ib})^{-1}$ which results in

$$Au_b=Bt_i+t_b \tag{4-9}$$

where

$$A=(G_{bb}-H_{bi}H_{ii}^{-1}G_{ib})^{-1}(H_{bb}-H_{bi}H_{ii}^{-1}H_{ib})$$

$$B=(G_{bb}-H_{bi}H_{ii}^{-1}G_{ib})^{-1}(G_{bi}-H_{bi}H_{ii}^{-1}G_{ii})$$

The matrices of the above equations are known except for the interfaced traction t_b and the interfaced displacement u_b. So Equation (4-9) will be used to assemble the system equation for the complete structure. For example, Equation (4-9) for the substructures k and k+1 is written in the following forms:

$$A^k u_b^k=B^k t_i^k+t_b^k+t_b^{k,k+1} \tag{4-10}$$

and

$$A^{k+1} u_b^{k+1}=B^{k+1} t_i^{k+1}+t_b^{k+1} \tag{4-11}$$

where $t_b^{k,k+1}$ is the external traction at the interface. Summing Equations (4-10) and (4-11) produces

$$A^k u_b^k+A^{k+1} u_b^{k+1}=B^k t_i^k+B^{k+1} t_i^{k+1} +t_b^k+t_b^{k+1}+t_b^{k,k+1} \tag{4-12}$$

If the above equation satisfies the compatibility and equilibrium conditions, $u_b^k=u_b^{k+1}$ and $t_b^k+t_b^{k+1}+t_b^{k,k+1} = t_b^{k,k+1}$, then the final system equation for substructures k and k+1 is written as

$$(A^k+A^{k+1})u_b^k=B^k t_i^k+B^{k+1} t_i^{k+1}+t_b^{k,k+1} \tag{4-13}$$

or

$$(A^k + A^{k+1})u_b^k = T_b^{k,k+1} \qquad (4\text{-}14)$$

where $T_b^{k,k+1}$ is the combination of external tractions acting at the interface and boundary reactions between substructure k and k+1.

The system equation in terms of interfaced displacements for the complete structure can be written as

$$A_b U_b = T_b \qquad (4\text{-}15)$$

The displacement vector U_b is expanded into a column substructure displacement vector u_b^k, in the order in which they appear in each substructure. Where A_b, T_b are obtained by placing the submatrices A^k and $T_b^{k,k+1}$ of each substructure respectively in their correct positions corresponding to U_b and summing all the overlapping terms with the elimination of a sufficient number of displacements to restrain rigid body degrees of freedom for the complete structure. Therefore the unknown interfaced displacement U_b can be calculated. When the substructure stiffness matrices A^k are assembled into the larger stiffness matrix A_b for the complete structure, their relative positions in this larger matrix depend on the sequence in which the individual boundary displacements are selected in Equation (4-9). Since some of the substructures will not be physically connected, this means that their coupling stiffness matrices will be equal to zero. As the coupling matrices occur only on substructures which have common boundaries; it is therefore advantageous, when selecting numbering systems for

substructures and displacements, to ensure that the component submatrices of A_b would occur arround the principal diagonal matrix.

Once the interfaced displacements u_b of each substructure are computed, the interfaced tractions t_b of each substructure are calculated by Equation (4-9), that is

$$t_b = Au_b - Bt_i \tag{4-16}$$

The noninterfaced displacements u_i are derived from Equation (4-3) in the following form

$$u_i = H_{ii}^{-1}(G_{ii}t_i + G_{ib}t_b + H_{ib}u_b) \tag{4-17}$$

Having determined the boundary displacements and tractions for each substructure, the interior stresses and displacements can be calculated independently for each substructure.

4.3 Description of the Computer Program Using Substructuring Analysis

The computer program for the substructuring analysis has been developed in terms of the mathematical formulation introduced above. The basic procedure used in the program is:

(1) Generation of input data to define the geometry of the boundary elements for each substructure.

(2) Integration of kernel shape function products to generate the system matrices for each substructure.

(3) Rearrangement of the system equation to get a new equation in terms of interfaced displacements.

(4) Solution of the assembly equation of the complete structure to get interfaced displacements.

(5) Calculation of interfaced tractions and interior information by obtaining interfaced displacements.

A brief flow diagram of the computer program is shown in Figure 4-1. The main program SUBBEM calls subroutine GAUSS, XINPU, XBEMAT, XFGBI, XSYSEQ, XSOL, XBSD and XBIPT. Subroutine GAUSS forms the weights and integration points of Gaussian formulae. Subroutine XINPUT reads the data defining the geometry, boundary conditions and material properties of each substructure.

Subroutine XBEMAT sets up the coordinates of the boundary nodes for point collocation and calls subroutine DINTEG to calculate the G and H matrices for each substructure. Subroutine DINTEG and SINTEG have the same functions as described in the last chapter. Subroutine XFGBI partitions the system equation for each substructure. Subroutine XSYSEQ forms Equation (4-9) for each substructure. Subroutine XSOL assembles the final system equation for the complete structure and calculates interfaced displacements and tractions for each substructure. Subroutine XBSD transforms the boundary

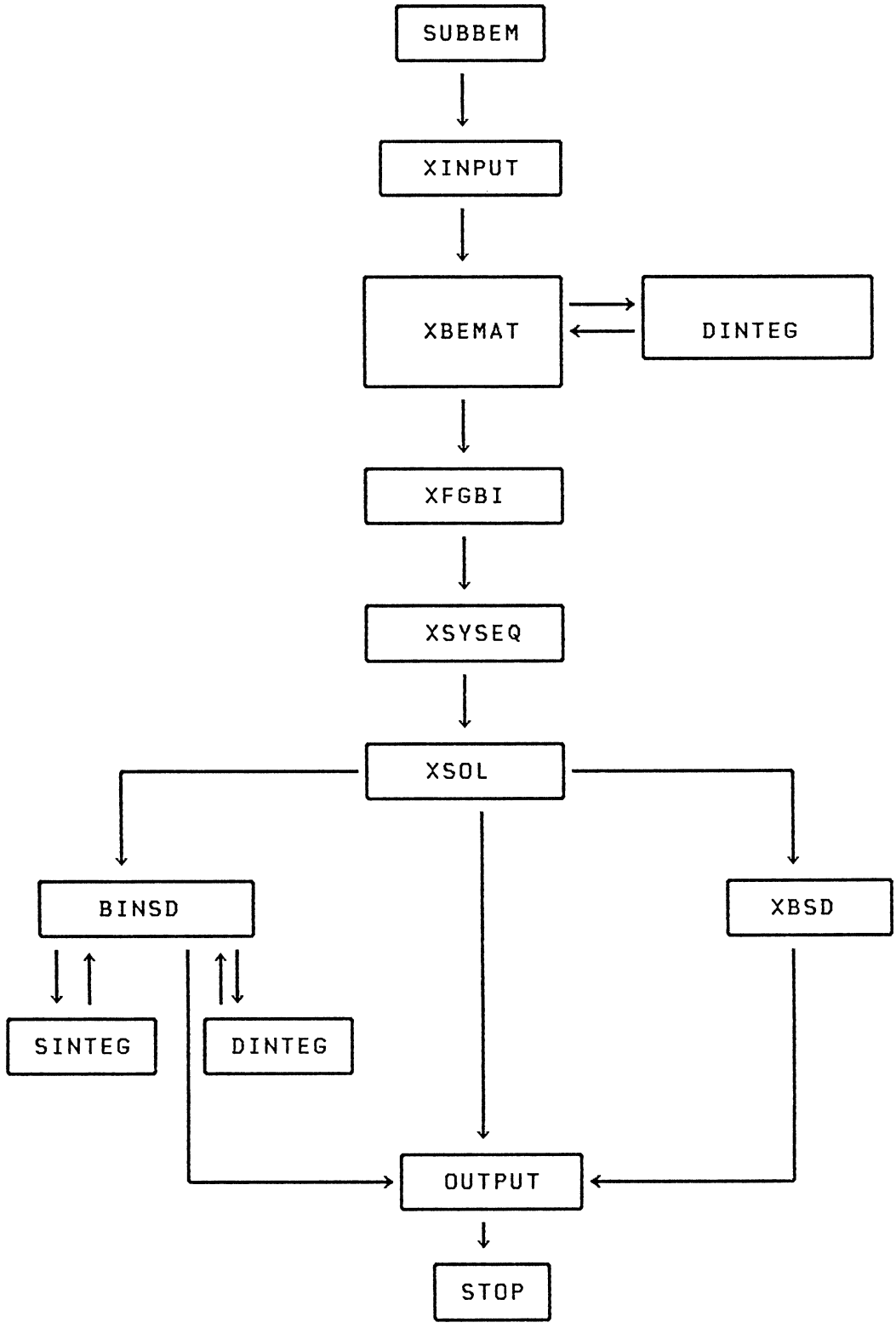

Figure 4-1 Brief Flow Diagram of the Substructuring Analysis by the Boundary Element Method

traction to boundary stresses and calculates interior information for each substructure.

4.4 Numerical Examples

Three examples have been chosen to test the SUBBEM program and confirm the mathematical formulation. The numerical results from the substructuring analysis are compared to the solutions of whole structural analysis by the boundary element method and the finite element method. The examples are:

(1) A two-dimensional beam which has different materials in zones under axial load.

(2) Bending of a two-dimensional beam under uniform load.

(3) Bending of a three-dimensional cantilever beam under end load.

4.4.1 A Two-dimensional Beam Which Has Different Materials in Zones under Axial Load.

The geometry and loading of the problem are shown in figure 4-2. The material properties of the beam are different in each zone. Sections 1 and 3 have the same material properties with elastic modulus $E=3.0\times10^7$ psi. The

elastic modulus of substructure 2 is 1.0×10^7 psi. The Poisson ratio is assumed to be zero in all regions.

The problem was divided into three substructures matching the three different regions. The boundary of each substructure was discretized by using 6 isoparametric quadratic boundary elements (Figure 4-3). The whole beam was discretized by 6 isoparametric 8-node quadratic finite elements (Figure 4-4).

The conventional boundary element method could not be used to solved the problem because of the different material properties in zones. The solutions of the substructuring analysis by the boundary element method produced the correct answer as did the finite element solution (Table 4-1). As seen from Figure 4-3, the substructuring analysis has the capability of solving the zoned body problems and providing additional interior information as compared to the conventional boundary element method.

It was assumed that there was a uniform load, q=1 (lb/in) acting on the cross-section x=2 (in) in the positive x-direction. The solution for the problem using the substructuring analysis were found to be correct (Table 4-2). This means that the substructuring analysis by the boundary element method can solve the problem with a load applied in the domain.

4.4.2 Bending of a Two-dimensional Beam under Uniform Load.

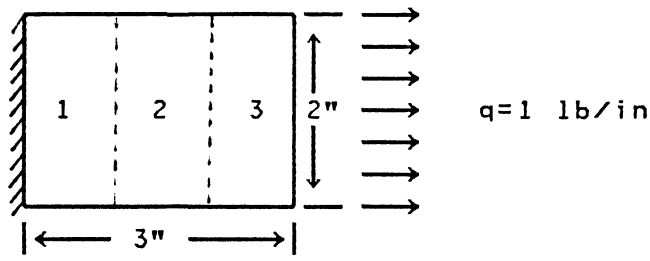

Figure 4-2 A Two-dimensional Beam Which Has Different Materials in Zones under Axial Load

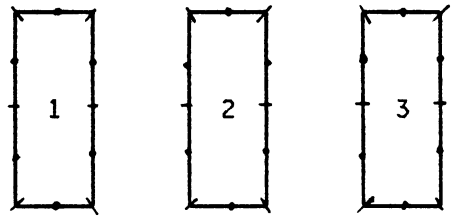

Figure 4-3 Substructuring Model of the Beam

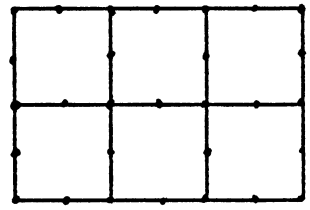

Figure 4-4 The Finite Element Model of the Beam

Table 4-1 Comparison of Deflections and Stresses for a Zoned Beam under Uniform Tension

method	at point (1,1)		at point (2.5,1)	
	σ_{xx} psi	u_x x10^{-7} in	σ_{xx} psi	u_x x10^{-7} in
exact solution[a]	1.00000	0.3333	1.00000	1.5000
SUBBEM	1.00000	0.3333	1.00000	1.5000
FEM	1.00000	0.3333	1.00000	1.5000

[a] Beer and Johnston 1981

Table 4-2 Comparison of Deflections and Stresses for a Zoned Beam under Uniform Tension and Interior Loading

method	at point (1,1)		at point (2.5,1)	
	σ_{xx} psi	u_x x10^{-7} in	σ_{xx} psi	u_x x10^{-7} in
exact solution[a]	2.00000	0.6667	1.00000	2.8333
SUBBEM	2.00000	0.6667	1.00000	2.8333
FEM	2.00000	0.6667	1.00000	2.8333

[a] Beer and Johnston 1981

The uniformly loaded beam has the same dimensions and boundary conditions as those in the problem discussed in Section 3.6.2 . The beam was divided into 3 substructures for this analysis. The boundary of each substructure was discretized using 8 isoparametric quadratic elements (Figure 4-5) and 16 isoparametric quadratic elements (Figure 4-6).

Comparison of the stress and displacement at point A calculated by using substructuring analysis with that obtained from the conventional boundary element method is shown in Table 4-3 . The results show close agreement between these two methods. The substructuring analysis reduces the computational time as the number of nodes increases. Moreover, if the dimensions and loading of substructure 3 change , we don't have to recalculate the coefficient matrices for the other two substructures during the reanalysis of the problem which can save two-thirds of the computer time. This is an important point in the following structural shape optimization.

4.4.3 Bending of a Three-dimensional Catilever Beam under End Load.

The beam has the same dimensions and boundary conditions as those in the problem discussed in Section 3.6.3 . Three analyses have been carried out using the boundary element method. The whole structural analysis of

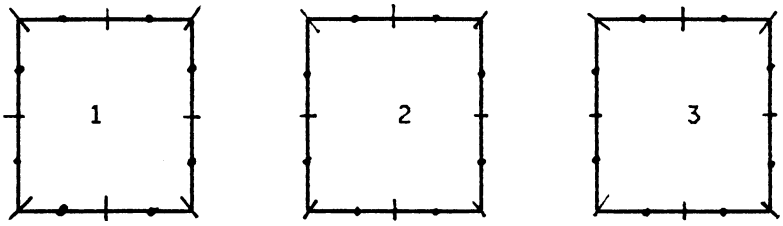

Figure 4-5 Eight Elements on Each Substructure for a Simply Supported Beam

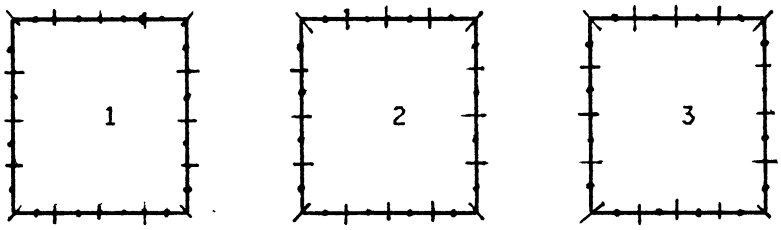

Figure 4-6 sixteen Elements on Each Substructure for a Simply Supported Beam

Table 4-3 Comparison of Deflection , Stress and Computer Time for a Simply Supported Beam under Uniform Load

method	logitudinal stress σ_{xx} psi	vertical deflection u_y x10^{-6} in	CPU time (sec)
exact solution[a]	6.95	.508	-----
BEM (16 ele.)	7.01	.503	6.50
BEM (32 ele.)	6.957	.505	32.43
SUBBEM (24 ele.)	7.013	.502	7.70
SUBBEM (48 ele.)	6.933	.504	26.64

[a] Timoshenko and Goodier 1970

the problem is modeled by 18 isoparametric quadratic quadralateral elements (Figure 4-7). In substructural analysis, the beam was divided into two and three substructures as shown in Figures 4-8 and 4-9 respectively. In Figure 4-8, the boundary of each substructure was dicretized using 10 isoparametric quadratic quadralateral elements. In Figure 4-9, the boundary of each substructure was discretized using 6 isoparametric quadratic quadralateral elements.

Table 4-4 shows the results of the different analyses. The substructural method not only reduced the computational time but also improved the solution accuracy over that obtained without the subdivision.

4.5 Conclusion

The computer program for substructuring analysis by the boundary element method has been developed using isoparametric quadratic line and quadralateral boundary elements. The results for practical problems of two- and three-dimensional elasticity have been successfully solved. As seen from the numerical examples of the last section we can summarize the following advantages and disadvantages of substructuring analysis as opposed to whole structural analysis.

Advantages:

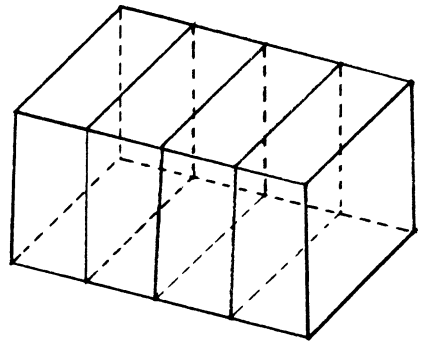

Figure 4-7 Eighteen Elements on a Whole Beam

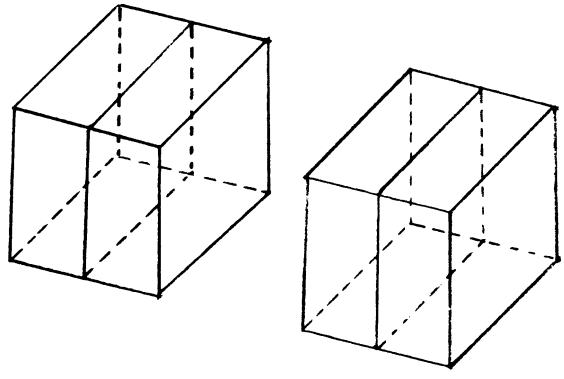

Figure 4-8 Ten Elements on Each Substructure of a Three-dimensional Beam

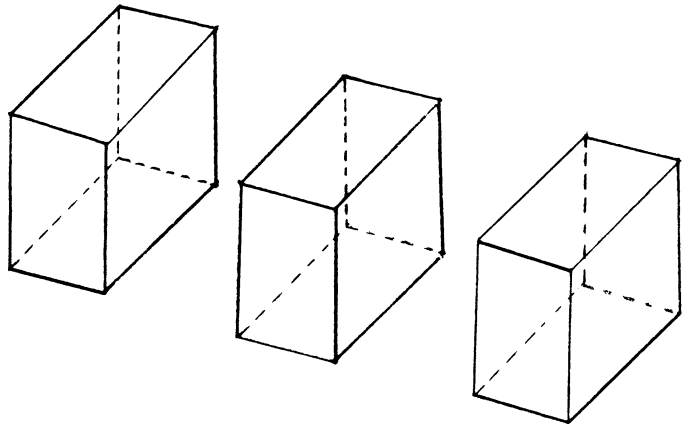

Figure 4-9 Six Elements on Each Substructure of a Three-dimensional Beam

Table 4-4 Comparison of Deflection and Stress for a Cantilever Beam under End Load

method	deflection u_y at free end (in)	stress σ_{xx} at y=2 in , x=2 in (psi)	CPU time (sec)
exact solution[a]	-7.616×10^{-2}	6.000	------
BEM (18 ele.)	-7.469×10^{-2}	6.110	105.4
SUBBEM(2 subs.)	-7.645×10^{-2}	6.111	97.0
SUBBEM(3 subs.)	-7.589×10^{-2}	6.096	59.2

[a] Brebbia 1982

(1) Reduced computer time and improved solution accuracy.

(2) The problem having different material properties in different zones can be solved.

(3) Loading not on the boundary can be applied

(4) The final system equation can be formulated once. Only slight changes in the coefficient matrix are necessary for the portion of the modified substructures during the optimization process.

Disadvantages:

(1) More input data and more set up time is required.

CHAPTER 5

COMBINING THE BOUNDARY ELEMENT METHOD WITH OPTIMIZATION

5.1 Introduction

Shape optimization problems seek the best boundary layout of structures or structural elements. The boundary element method provides the capability and advantages of modeling the varied shape of the boundaries during the optimization process. Because the boundary element method only models the boundary, it is possible to obtain a good representation of the boundary. Also, the shape of the boundary may easily be coupled with a general shape function.

In the papers concerned with shape optimization, the design variables have often been the nodal coordinates of the finite element model. Such a choice exhibits many severe drawbacks which are: a large number of design variables, poor boundary representation, and the difficulty of maintaining an adequate finite element mesh during the optimization process. Imam 1982, and Braibant and Fleury 1984 introduce a shape function to represent the boundary and consider independent shape variables as the design

variables. The design variables have been reduced, but the difficulty of the finite element mesh refinement is still present. In this chapter, the region of structure that is to be modified during the optimization process is defined by one or more design patches which contain a portion of the boundary elements. The shape of the design patch is generated by a Bezier or B-spline technique and discretized by the boundary element mesh.

5.2 Method of Optimization

Mathematically, the structural optimization problem can be stated as

$$\text{minimize} \quad f(\bar{x}); \quad \bar{x}=[x_1, x_2, x_3, \ldots\ldots x_N]^T \in R^N \qquad (5\text{-}1)$$

$$\text{subject to} \quad \Phi_k(\bar{x}) \geq 0 \quad k=1,2,3,\ldots.K \qquad (5\text{-}2)$$

$$\Psi_l(\bar{x}) \equiv 0 \quad l=1,2,3,\ldots.L \qquad (5\text{-}3)$$

where

$\bar{x}$ = a column vector of design variables.

N = total number of design variables.

$f(\bar{x})$ = the design criteria or objective function.

$\Phi_k(\bar{x})$ = K inequality constraint functions. These functions delimit regions in the design space.

$\Psi_l(\bar{x})$ = L equality constraint functions. These functions vastly reduce the number of candidate

designs, because they require specific combinations of the design variables.

The main goal of designing efficient structures, has been to minimize weight as the objective function. Other quantities, such as deflection, stiffness, energy, stress concentration and actual cost, have also been used as objective functions.

Design variables may be cross-sectional variables or other parameters which describe the structural configuration and the material properties. In shape optimization, the configuration parameters are nodal coordinates or control nodes of the shape function.

Constraints are generally restrictions that must be satisfied for the design to be acceptable or feasible. Constraints may be of two types. Equality constraints are mostly behavioral constraints such as equilibrium, compatibility, and constitutive relations. Inequality constraints usually represent limitations imposed on the stresses, deflections, etc. A particular kind of inequality constraint is a side constraint or bound which imposes a direct limit on the range of variation of a design variable.

In general, for structural shape optimization problems only certain explicit constraints are simple linear functions of the design variables, and both the objective function and implicit constraints (usually concerned with stresses and/or displacements in the structure) are dependent in a nonlinear manner on the design variables.

The solution of such nonlinear structural optimization problems requires a special mathematical programming algorithm. The optimization code OPT has been used for solving the optimization problem. OPT is a program employing the generalized reduced gradient technique and was developed by Gabriele and Ragsdell 1976. The generalized reduced gradient method is introduced as following from Gabriele and Ragsdell 1976.

With no loss of generality, the optimization problem (equation 5-1 through 5-3) can be transformed into the following form which is handled by the reduced gradient method.

$$\text{Minimize} \quad f(\bar{x}); \ \bar{x}=[x_1, x_2, x_3, \ldots\ldots x_N]^T \in R^N \qquad (5\text{-}4)$$

$$\text{Subject to} \ \Psi_m(\bar{x}) \equiv 0 \quad m=1,2,3,\ldots.M \qquad (5\text{-}5)$$

$$A \leq x \leq B \qquad (5\text{-}6)$$

The Nx1 vectors A and B represent the upper and lower bounds on the design variables. The inequality constraints of (5-2) are included as equality constraints by using the following transformation,

$$\Psi_k(\bar{x})=\Phi_k(\bar{x})-S_k \equiv 0 \qquad (5\text{-}7)$$

$$0 \leq S_k \leq \infty \qquad k=1,2,3,\ldots.,K$$

The variables S_k are nonnegative slack variables included in the original set of design variables. Hence, N now represents the total number of design variables plus the number of slack variables included to transform the inequality constraints. The parameter M represents the total number of constraints, equality and inequality. The

constraints considered in (5-5) include only functional constraints, variables bounds are contained in (5-6) and are handled separately.

Consider the following strategy. Divide the design vector $\bar{x}$ into two classes, (1) decision variables, and (2) state variables,

$$\bar{x} = [\bar{z}, \bar{y}]^T \tag{5-8}$$

$$z = [z_1, z_2, z_3, \ldots\ldots z_Q]^T \text{; decision variables} \tag{5-9}$$

$$y = [y_1, y_2, y_3, \ldots\ldots y_M]^T \text{; state variables} \tag{5-10}$$

$$Q = N-M \tag{5-11}$$

The decision variables are independent, and the state variables are slaves to the decision variables used only to satisfy the constraints.

Let us examine the first variation of $f(\bar{x})$ and $\Psi(\bar{x})$,

$$df = g(\bar{z})^T \, d\bar{z} + g(\bar{y})^T \, d\bar{y} \tag{5-12}$$

$$d\Psi = \frac{\partial \Psi}{\partial \bar{z}} \, d\bar{z} + \frac{\partial \Psi}{\partial \bar{y}} \, d\bar{y} \equiv 0 \tag{5-13}$$

where

$d\bar{z}$ = Qx1 vector of differential displacements of $\bar{z}$,

$d\bar{y}$ = Mx1 vector of differential displacements of $\bar{y}$,

$g(\bar{z})$ = Qx1 vector of gradients of the objective function with respect to $\bar{z}$

$g(\bar{y})$ = Qx1 vector of gradients of the objective function with respect to $\bar{y}$

$\partial\Psi/\partial\bar{z}$ = MxQ matrix of gradients of the constraints with rspect to $\bar{z}$

$\partial\Psi/\partial\bar{y}$ = MxM matrix of gradients of the constraints with rspect to $\bar{y}$

Solving (5-13) for $d\bar{y}$ yields,

$$d\bar{y} = - \frac{\partial\Psi^{-1}}{\partial\bar{y}} \frac{\partial\Psi}{\partial\bar{z}} d\bar{z} \qquad (5\text{-}14)$$

Substituting (5-14) into (5-12) and rearranging will yield the following linear approximation to the reduced gradient

$$g_r(\bar{x})^T = g(\bar{z})^T - g(\bar{y})^T \frac{\partial\Psi^{-1}}{\partial\bar{y}} \frac{\partial\Psi}{\partial\bar{z}} \qquad (5\text{-}15)$$

The generalized reduced gradient is the rate of change of the objective function with respect to the decision variables with the state variables adjusted to maintain feasibility. The word "generalized" is included to underscore the presence of nonlinear constraints. When the constraints are linear the state variable adjustment is significantly simplified. Geometrically the reduced gradient can be described as a projection of the original N dimensional gradient onto the Q dimensional feasible region described by the decision variables. Hence the reduced gradient can be used in the same manner as a conventional gradient algorithm to search for a minimum of $f(\bar{x})$ in the reduced space. The state variables are adjusted during the course of the search to maintain feasibility.

From the discussion above, it is easy to see that an advantage of using the generalized reduced gradient method for constrained problems is the use of state variables to

satisfy the constraints. To submit a problem to OPT the user must supply three basic elements, (1) a function subprogram defining the objective function, (2) a subroutine defining the constraints, and (3) a calling program. In this shape optimization, the design objective is to minimize the weight or the peak stress of a structural component, subject to geometry, displacement and stress constraints. The B-spline or Bezier method is introduced to describe the shape of the design. The control points on these curves are the design variables. The detailed optimization process is discussed in section 5.4 .

5.3 Selection of Shape-Design Function

The shape-design functions of the modified boundary are selected by using the blending functions of the Bezier or the B-spline technique. The shape of the design patch is determined by the locations of control points and the blending functions. The design patch may include several boundary elements. Therefore the design variables are no longer the position of the nodes of the boundary elements, but the points which control the shape of the design patch.

The characteristics of the Bezier methods and the B-spline methods are briefly shown as follows:

Bezier methods:

The mathematical form of the Bezier curves are

$$P(u)=\sum_{j=0}^{n} p_j B_{j,n}(u) \qquad (5\text{-}16)$$

where $B_{j,n}(u)$ is a blending function

$$B_{j,n}(u)=C(n,i)u^j(1-u)^{n-j}$$

$C(n,i)$ is the binomial coefficient

$$C(n,i)=N!/(i!(n-i)!)$$

p_j is the location of the control point

u is the influence parameter $0 \le u \le 1$

Figure 5-1 shows an example of a planar Bezier curve. The curve shown uses five control points. The formulation of the Bezier curve extends easily to describe three-dimensional surfaces by generating the cartesian product of two curves. Two similar blending functions are used, one for each parameter:

$$P(u,v)=\sum_{i=0}^{n}\sum_{j=0}^{m} p_{j,j} B_{j,n}(u) B_{j,m}(v) \qquad (5\text{-}17)$$

B-spline methods

The mathematical form of the B-spline curve is

$$P(u)=\sum_{i=0}^{n} p_j N_{j,k}(u) \qquad (5\text{-}18)$$

where $N_{j,k}(u)$ is the B-spline blending function of degree k-1 which may be defined recursively as follows:

$$N_{j,1}(u)=1 \quad \text{if } t_j \le u \le t_{j+1}$$

$$0 \quad \text{otherwise}$$

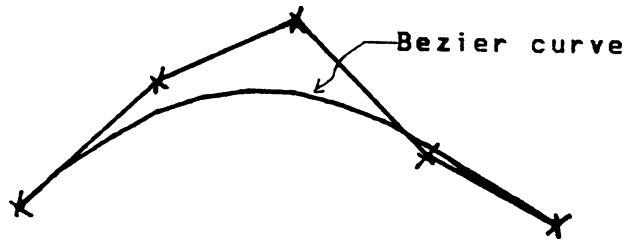

Figure 5-1 A Bezier Curve and the Five Control Points Used to Define It

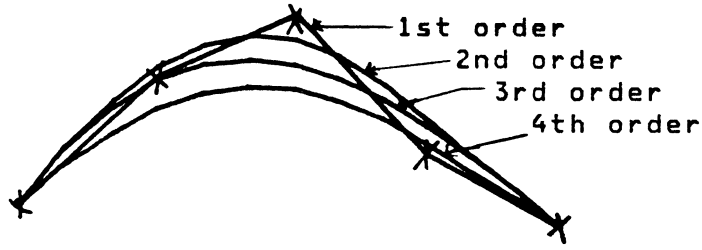

Figure 5-2 Several B-spline Curves Derived From Five Control Points. Each of the Four Curves has a Different Order.

$$N_{i,k}(u)= \frac{(u-t_i)N_{i,k-1}(u)}{t_{i+k-1}-t_i} + \frac{(t_{i+k}-u)N_{i+1,k-1}(u)}{t_{i+k}-t_{i+1}} \quad (5\text{-}19)$$

Knot values t are chosen with the following rule:

$t_i = 0$ if $i \leq k$

$= i-k+1$ if $k \leq i \leq n$

$= n-k+2$ if $i > n$

The parameter u varies from 0 to n-k+2

Figure 5-2 shows an example B-spline curve in the plane. The B-spline curves were derived from five control points. Each of the three curves has a different order. B-splines extend to describe surfaces by the same cartisian product method used with Bezier curves:

$$P(u,v)= \sum_{i=0}^{n} \sum_{j=0}^{m} p_{i,j} N_{i,k}(u) N_{j,l}(v) \quad (5\text{-}20)$$

The B-splines have the same characteristics as the Bezier curves: the control points affect curve shape in a natural way and the curve is variation diminishing, axis-independent and multivalued. The main advantages of the B-splines are first that local control of the curve shape can be achieved by using a set of blending function that have local support only, and second that additional control points can be introduced without increasing the degree of the curve. B-splines offer more parameters to the designer than Bezier curves: the degree can be selected, as well as the multiplicities of control points or knots.

The formulation of Bezier and B-spline methods is easily extended to the generation of a modified shape. Once the new shape has been created, the boundary element mesh may be updated and the stresses and displacements on the boundary and/or selected interior points may be calculated.

5.4 The Process of Optimization

The region of the structure that is to be modified during the optimization process is defined by one or more design patches which contain a portion of the boundary elements. The curve of the design patch is generated by a B-spline curve. The change in geometry within a boundary element in the design patch for two-dimensional problems is described by the following equation.

$$\begin{Bmatrix} x' \\ y' \end{Bmatrix} = \begin{Bmatrix} x \\ y \end{Bmatrix} + \begin{Bmatrix} \Delta x \\ \Delta y \end{Bmatrix} = \sum_{i=1}^{I} N_i(\eta) \begin{Bmatrix} x_j \\ y_j \end{Bmatrix} + \sum_{j=0}^{J} B_{j,k}(u) \begin{Bmatrix} v_{xj} \\ v_{yj} \end{Bmatrix} \qquad (5\text{-}21)$$

where

x, y are initial coordinates in direction x, y respectively.

x', y' are the updated coordinates.

x_j, y_j are the i th nodal coordinate of each boundary element.

J+1 is total number of control points.

I is total number of nodes per element.

N_i are the corresponding shape functions described earlier.

η is the local coordinate of each element.

u is the influence parameter.

$B_{j,k}$ is a blending function of B-spline or Bezier curve , subscript k is the order of continuity of the curve.

The relation

$$\begin{Bmatrix}\Delta x\\ \Delta y\end{Bmatrix} = \sum_{j=0}^{J} B_{j,k}(u)\begin{Bmatrix}v_{xj}\\ v_{yj}\end{Bmatrix} \qquad (5\text{-}22)$$

forms the mathematical expression for the changes in the design patch geometry. Δx and Δy are defined by the n+1 blending functions $B_{j,k}$ whose coefficients are the variations v_{xj} and v_{yj} of the n+1 vertices of the design patch which are taken as design variables. The variations of design variables v_{xj} and v_{yj} are represented in directions x and y respectively. Once the new shape has been created, the boundary element mesh may be updated and the stresses and displacements on the boundary and/or selected interior points may be calculated by the boundary element method.

The change of geometry within a boundary element in the design patch for a three-dimensional problem is described by the following equation.

$$\begin{Bmatrix}x'\\ y'\\ z'\end{Bmatrix} = \sum_{i=1}^{I} N_i(\eta_1,\eta_2)\begin{Bmatrix}x_j\\ y_j\\ z_j\end{Bmatrix}$$

$$+\sum_{j=0}^{J}\sum_{m=0}^{M} B_{j,k}(u_x)B_{m,l}(u_y)\begin{Bmatrix} v_{xj} \\ v_{yj} \\ v_{zj} \end{Bmatrix} \qquad (5\text{-}23)$$

The stresses and displacements are calculated for every new design shape by the full boundary element method and the gradients of the stress and displacement are evaluated by the finite difference technique using the results of the boundary element method.

Separate analyses for each design variable v_j for the approximation of $\partial\sigma_i/\partial v_j$, $\partial u_i/\partial v_j$ by a finite difference expression is an obvious possibility for computing gradients, but such an operation would require J+1 complete analyses at each iteration. This can be avoided by differentiating the system equation (Equation 3-15) with respect to v_j obtaining

$$\frac{\partial}{\partial v_j}([F]\{u\}-[G]\{t\})=0 \qquad j=1,2.....n \qquad (5\text{-}24)$$

$$\text{ie. } \frac{\partial[F]}{\partial v_j}\{u\}+[F]\begin{Bmatrix}\frac{\partial u}{\partial v_j}\end{Bmatrix}-\frac{\partial[G]}{\partial v_j}\{t\}-[G]\begin{Bmatrix}\frac{\partial t}{\partial v_j}\end{Bmatrix}=0$$

where

[F] and [G] are calculated from the first analysis of the problem.

{u} and {t} are known values from solutions of Equation (3-12).

$\partial[F]/\partial v_j$ and $\partial[G]/\partial v_j$ are calculated by the finite difference method due to the variation of v_j

n is the total number of design variables.

Equation (5-10) can be written in the following form in terms of unknown displacement gradients $\partial\{u\}/\partial v_j$ and traction gradients $\partial\{t\}/\partial v_j$.

$$[A]\begin{Bmatrix}\dfrac{\partial\{u\}}{\partial v_j}\\ \dfrac{\partial\{t\}}{\partial v_j}\end{Bmatrix}=\frac{\partial[G]}{\partial v_j}\{t\}+\frac{\partial[F]}{\partial v_j}\{u\}=\{f\}_j \quad j=1,2...n \qquad (5\text{-}25)$$

The problem has thus been reduced to solving Equation (5-7) with J right hand sides, $\{f\}_1,\{f\}_2,.....\ \{f\}_n$, which will consume only a fraction of the computer time needed for the method mentioned previously. Once the traction gradient with respect to the design variables v_j is obtained, this information is used at the element level to calculate the stress gradient with respect to v_j. The calculation of the boundary stress gradient is similar to the calculation of the boundary stress (Equation 3-15 to 3-17).

A brief flow chart of the process of optimization is illustrated in Figure 5-3. The main program MAIN initializes the program parameters and calls subroutine OPT and INPUT. Subroutine INPUT reads the data relating the geometry, boundary conditions, and material properties for the boundary element model. Subroutine OPT operates the process of optimization and calls the objective function

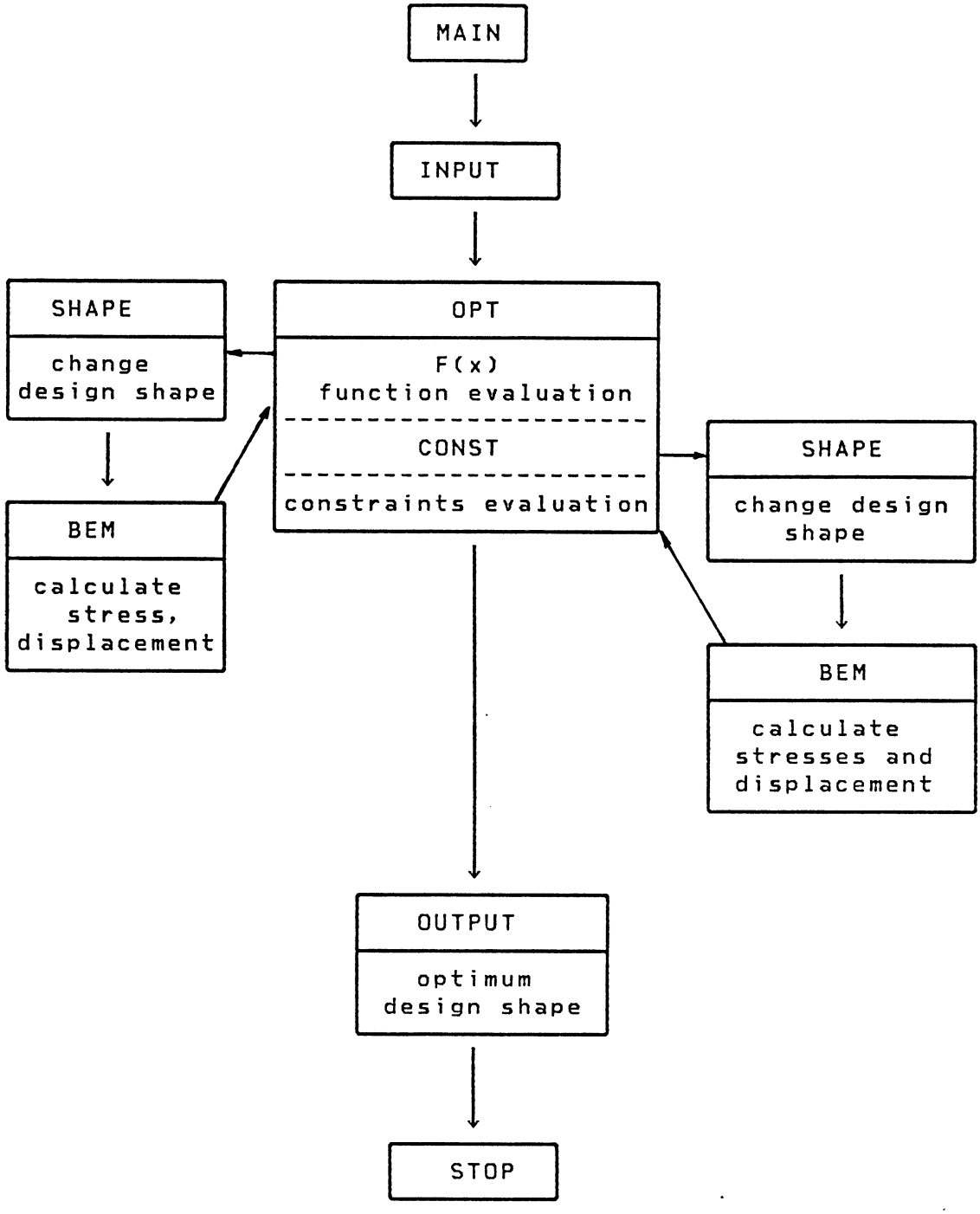

Figure 5-3 A Brief Flow Chart of the Optimization Process

F(x) and the constraint subroutine, CONST. Function F(x) calls subroutine SHAPE and/or BEM and also evaluates the value of the objective function. Subroutine CONST calls subroutine SHAPE and BEM, while evaluating the values of the constraints. Subroutine SHAPE forms new coordinates by the Bezier or B-spline method due to the change of design variables. Subroutine BEM solves the problem by the boundary element method. The OUTPUT shows the minimum value of the objective function and optimum design shape.

5.5 Applications of the Boundary Element Method for Structural Shape Optimization

Six examples were used for testing the optimization procedure:

(1) A square plate with a square hole under uniform tension.

(2) A thick wall pipe under internal pressure.

(3) Optimal shape design of a two-dimensional fillet.

(4) Optimal shape design of a ladle hook.

(5) Optimal tapering of a cantilever beam.

(6) Optimal shape design of a three-dimensional fillet.

5.5.1 A Square Plate With a Square Hole under Uniform Tension.

The initial geometry and loading for the problem is illustrated in Figure 5-4. The corner of the hole will lead to large local stresses. The design objective is to find the optimum shape of the hole which has the minimum peak stress on the boundary for specified dimensions of the hole and loading. Stress constraints are imposed which require the stress along the hole be less than the peak stress.

In the quarter portion of the plate (Figure 5-5), the region is modeled by 16 quadratic boundary elements. Edge AB is considered as a design patch which contains 4 elements (9 nodes). The curve of the design patch is represented by a 4th order Bezier curve or B-spline which has 5 control points. In this example, all control points are not required to be design variables, as they depend on the following cases for the design condition.

Now the optimization problem can be formulated as follows:

Minimize σ_{max}

$$\text{Subject to } (\sigma_{max}-(\sigma_j+\sum_{i=1}^{I}\frac{\partial\sigma_j}{\partial v_i}\delta v_i))/\sigma_{max}\geq 0 \quad j=1,2...n \qquad (5\text{-}26)$$

and $\quad c_i \geq v_i \geq d_i$

where

σ_{max} is the peak stress at point 1 or 5

σ_j are stresses at the jth node of the boundary element in the design patch

v_i are variations of the design variables.

n=9 is the total number of nodes in the design patch.

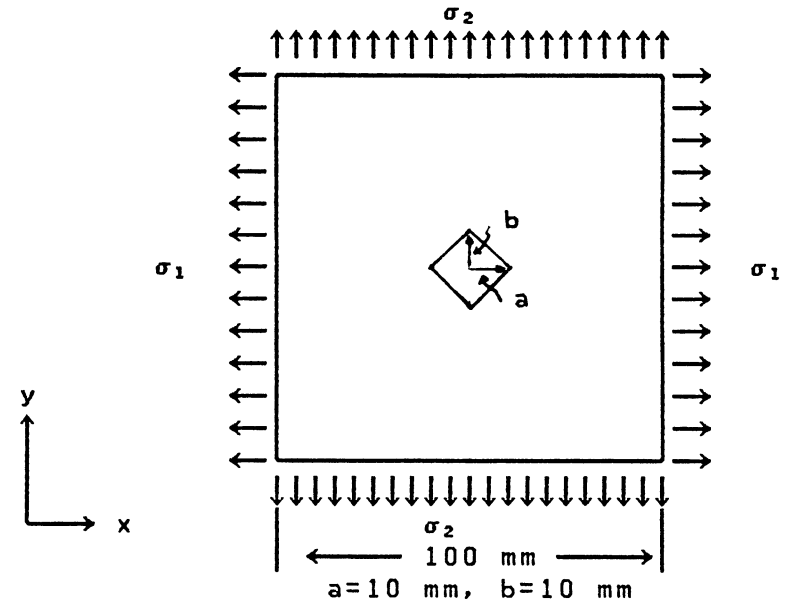

Figure 5-4 A Square Plate With a Square Hole under Uniform Tension

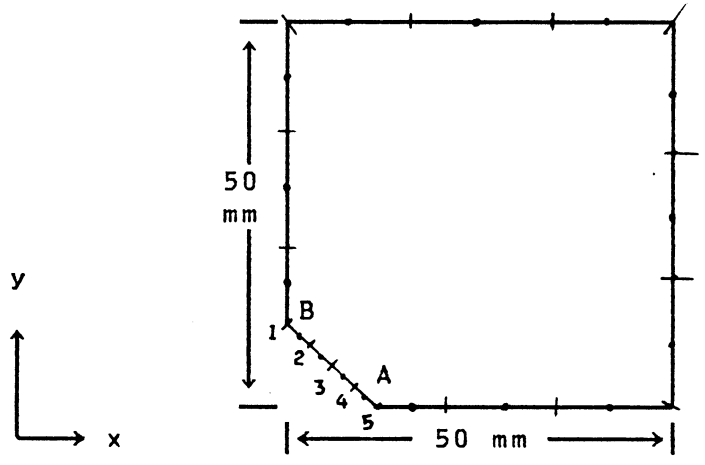

Figure 5-5 Boundary Element Mesh of the Quarter Portion of the Plate

I is the total number of the design variables.

c_i, d_i are the move limits imposed on the design variables.

There are three sets of design conditions based on different specified dimensions and loadings.

case(1): Control points 1 and 5 are fixed (a=10 mm, b=10 mm). Control points 2,3 and 4 are design control points, so there are six design variables (x and y position of each control point). The loadings for the problem are $\sigma_1=\sigma_2=120$ N/mm^2. The final results give a peak stress of 248.87 N/mm^2. The optimum shape of the hole (Figure 5-6) is a circle.

case(2): Control point 1 can be moved along the y-direction (i.e. 9 mm$\leq$b$\leq$30 mm). Control point 5 can be moved along the x-direction (i.e. 9 mm $\leq$a$\leq$30 mm). Thus there is a total of eight design variables. The loading for the problem is the same as for case (1). The final result produces a peak stress of 247.63 N/mm^2. The optimum shape of the hole (Figure 5-7) is almost a circle. The radius of the circle is close to 9 mm (a=9.05 mm, b=9.03 mm) which is the smallest diameter possible. The smallest hole in the plate has the lowest peak stress.

case(3): Control point 1 can be moved along the y-direction (i.e. 5 mm$\leq$b$\leq$30 mm). Control point 5 can be moved along the x-direction (i.e. 5 mm$\leq$a$\leq$30 mm). The

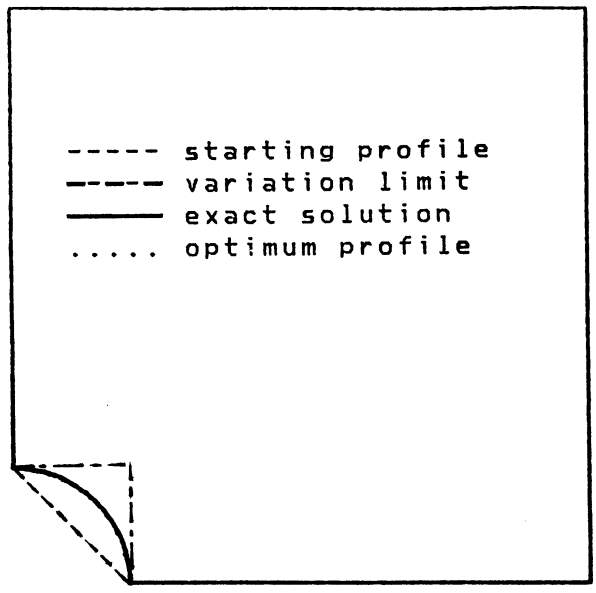

Figure 5-6 Optimum Shape of the Hole for Case 1

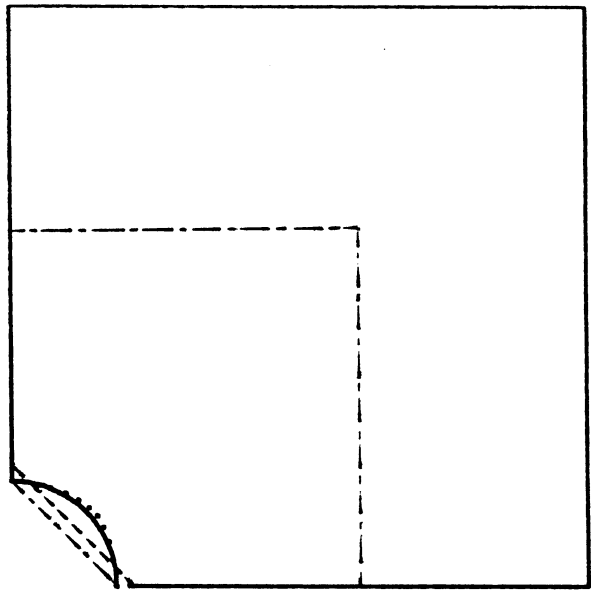

Figure 5-7 Optimum Shape of the Hole for Case 2

design variables for the problem are the same as for case (2). The loading of the problem is σ_1=120 N/mm^2 and σ_2=60 N/mm^2. The final result for the peak stress is 183.62 N/mm^2. The optimum shape of the hole (Figure 5-8) is an ellipse (where a=10.28 mm, b=5 mm).

The optimum shape has now been found, based on the assumption that the minimum peak stress in the plate is a constant tangential stress at the edge of the hole. The optimum shapes have been compared with the analytical shape in Figures 5-6 to 5-8. The numerical results for the peak stress and for the dimension of the hole are shown in Table 5-1. Both the peak stress and the optimum shape are very close to the analytical solution.

5.5.2 A Thick Wall Pipe under Internal Pressure

Case(1):

Figure 5-9 shows the initial cross-sectional geometry and loading for the problem. The design objective is to find the optimum shape of the outside boundary which has the minimum peak stress at the outside boundary, subject to a stress constraint on the inside boundary. One quarter of the section (Figure 5-10) has been modeled by 14 quadratic boundary elements. Edge AB is considered as a design patch which contains 4 elements (9 nodes). The curve of the design patch is represented by a 3rd order Bezier curve

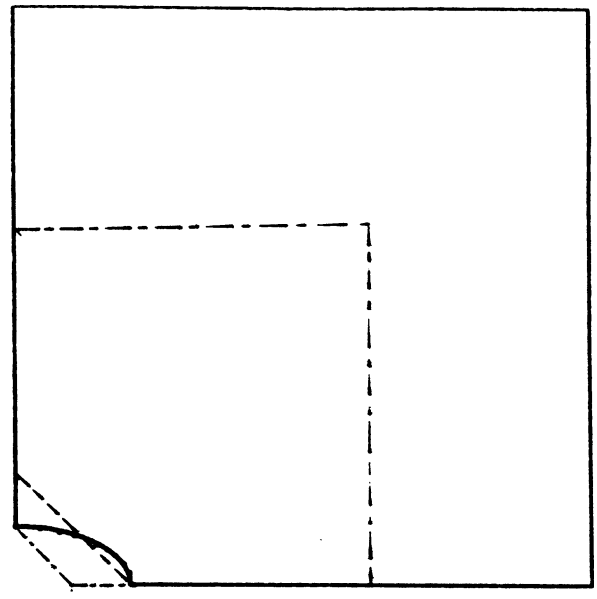

Figure 5-8 Optimum Shape of the Hole for Case 3

Table 5-1 Comparison of the Numerical Results With Analytical Solutions ($K=\sigma_{max}/\sigma_1$ is Stress Concentration Factor)

		numerical results		analytical results[a] for infinite plate		
case	σ_2/σ_1	b/a	K	b/a	K	shape of hole
case 1	1	1.000	2.074	1.0	2.0	circular
case 2	1	0.998	2.064	1.0	2.0	circular
case 3	0.5	0.486	1.530	0.5	1.5	ellipse

[a] Timoshenko and Goodier 1970

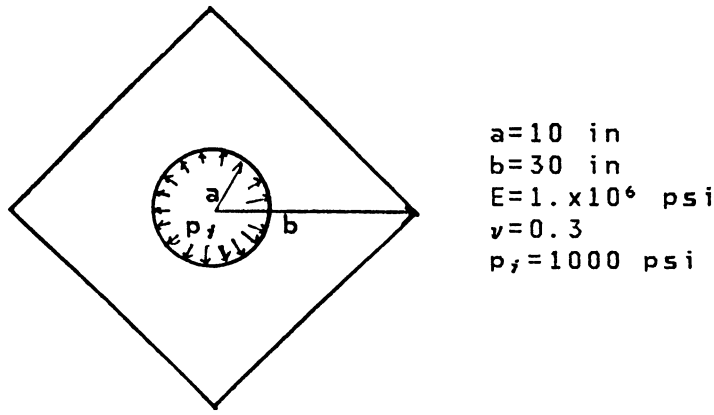

Figure 5-9 A Thick Wall Pipe under Internal Pressure for Case 1

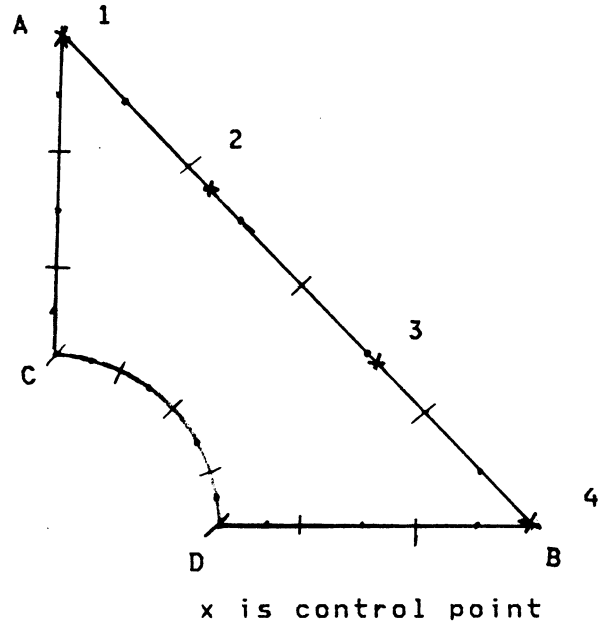

Figure 5-10 The Boundary Element Mesh for the Quarter Portion of the Pipe (Case 1)

which has 4 control points. Points 1 and 2 are fixed. Points 2 and 3 are active control points. So the resulting optimization problem has four design variables.

The formulation of the optimization problem is similar to Example 5.5.1

Minimize σ_e

$$\text{Subject to } (\sigma_0-(\sigma_j+\sum_{i=1}^{I}\frac{\partial\sigma_j}{\partial v_i}\delta v_i))/\sigma_0\geq 0 \quad j=1,2\ldots n \tag{5-27}$$

and $\quad c_i\geq v_i\geq d_i$

where

σ_e is the maximum stress on the edge AB

σ_0 =1250 psi inside tangential stress of the thick wall cylinder (inside diameter 2a=20 in, outside diameter 2b=60 in)

v_i are the variations of the design variables

σ_j are the stresses at the jth node of the boundary element at edge CD

I is the total number of design variables.

n=9 is the total number of nodes in the design patch

c_i and d_i are the move limits on the design variables

The numerical results produce a peak stress of σ_e=246.6 psi which is close to the exact value (250 psi) for the cylinder. The optimum shape almost matches the exact shape (Figure 5-11) for the thick cylinder which has constant tangential stress at both the inside and outside boundary.

Case(2):

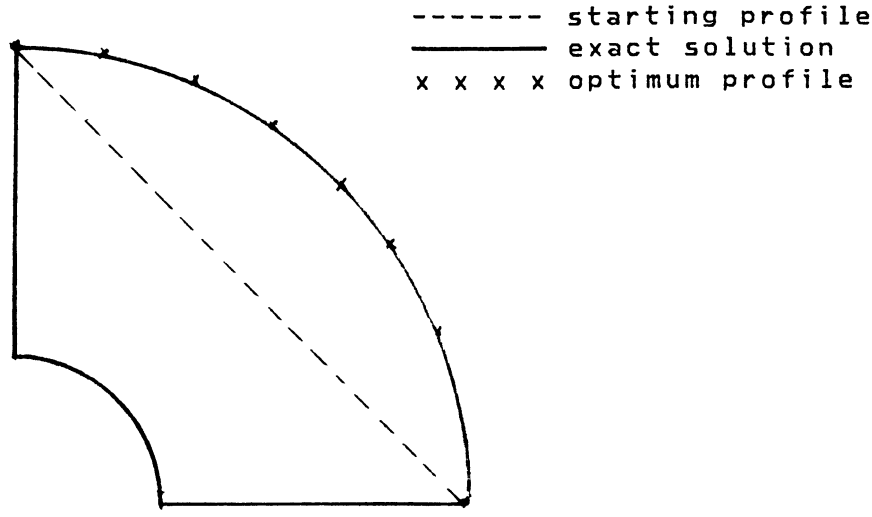

Figure 5-11 Optimum Shape for the Thick Wall Pipe for Case 1

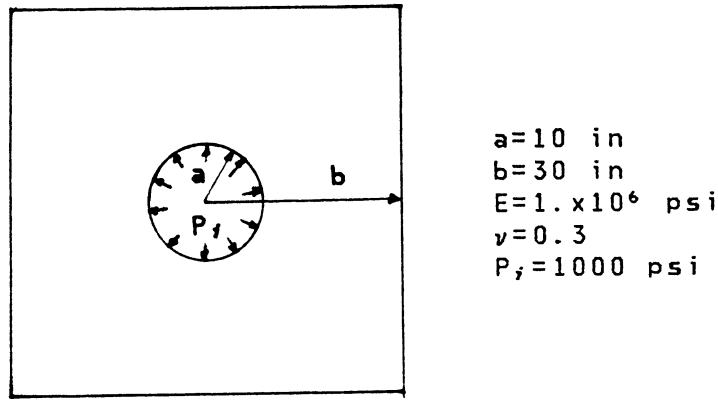

Figure 5-12 A Thick Wall Pipe under Internal Pressure for Case 2

The initial cross-sectional geometry and loading for the problem are shown in Figure 5-12. The design objective is to find the optimum shape of the outside boundary which has the minimum weight for the pipe, subject to stress constraints on the inside boundary. The boundary element model (Figure 5-13) and the formulation of the problem are similar to Case (1), but the design objective is the area of the quarter section.

The optimum cross-sectional area of 624.52 in^2 is close to the exact solution of 628.34 in^2 for the thick cylinder. The optimum shape (Figure 5-14) is also close to a circular shape for the thick cylinder.

5.5.3 Optimum Shape Design of a Two-dimensional Fillet.

The initial geometry and loading for the problem are shown in Figure 5-15. Only the upper section of the fillet is considered due to symmetry. The design objective is to find the optimum shape for edge AB to minimize the total area of the fillet. Stress constraints are imposed which require the stress along the edge AB to be less than a specified stress. The allowable stress for the problem was given three different values (135 psi, 125 psi and 115 psi) for three different cases.

The boundary of the problem is modeled by 21 quadratic boundary elements (Figure 5-16). Edge AB is considered as a design patch which contains 5 elements (11 nodes). The

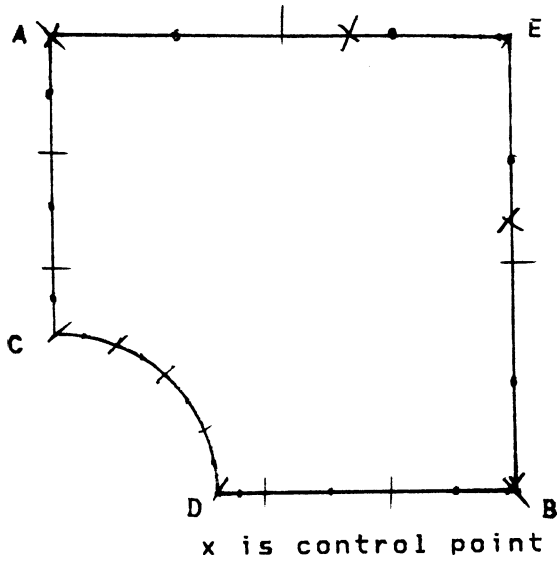

Figure 5-13 The Boundary Element Meshes for the Quarter Portion of the Pipe (Case 2)

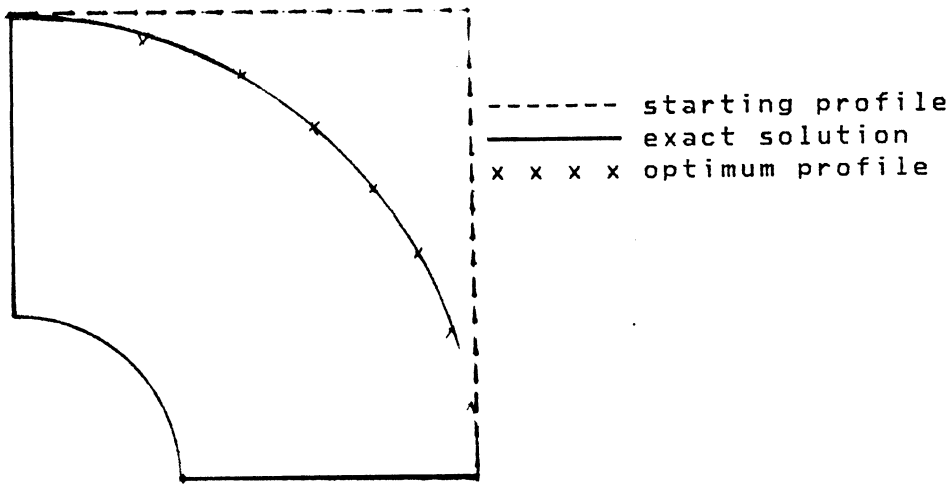

Figure 5-14 Optimal Shape for the Thick Wall Pipe for Case 2

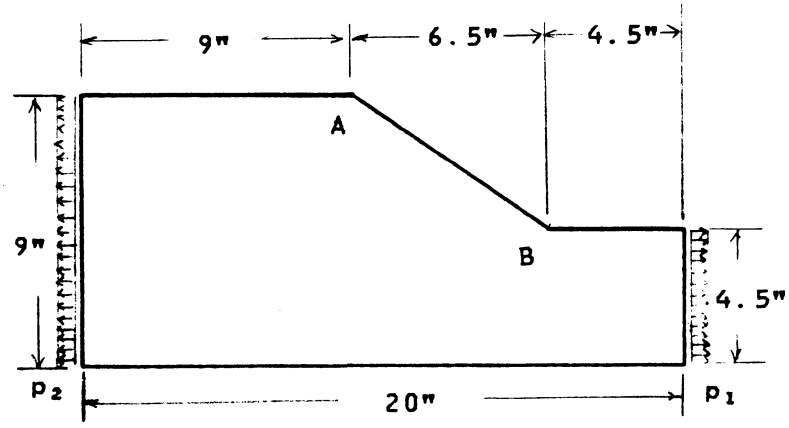

p_1=100 lb/in p_2=-50 lb/in

Figure 5-15 Upper Portion of the 2-D Fillet under Axial Loading

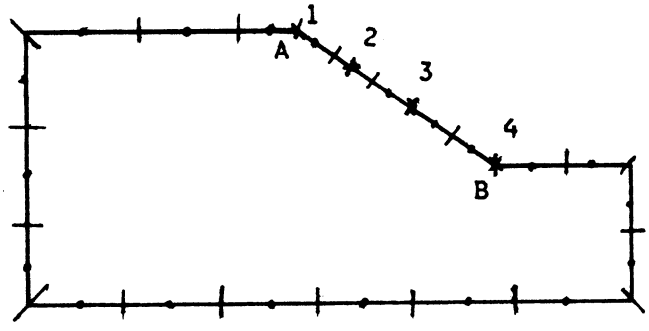

x is control point

Figure 5-16 The Boundary Element Mesh for the 2-D fillet

curve of the design patch is represented by a 4th order B-spline curve which has four control points. Points 1 and 4 are fixed. Points 2 and 3 are active control points, so there are a total of six design variables.

The formulation of the optimization problem is given as follows:

Minimize A

$$\text{Subject to } (\sigma_0 - (\sigma_j + \sum_{i=1}^{I} \frac{\partial \sigma_j}{\partial v_i} \delta v_i))/\sigma_0 \geq 0 \quad j=1,2...n \tag{5-28}$$

and $(x_j - 9)/9 \geq 0$

$(y_j - 4.5)/4.5 \geq 0$

and $c_i \geq v_i \geq d_i$

where

A is the area of the fillet

σ_0 is the specified stress (135 psi or 125 psi or 115 psi).

σ_j are stresses at the jth node of boundary elements in the design patch.

v_i are the variations of the design variables

I is the total number of design variables.

n=11 is the total number of nodes in the design patch

c_i and d_i are the move limits on the design variables

x_j and y_j are the coordinates of the design patch

Table 5-2 shows the results of the optimization. The higher the stress specified, the more the area is reduced. In Figure 5-17, the optimum shape is a continuous curve and

Table 5-2 Comparison of the Area of the 2-D Fillet for Different Allowable Stress Limits

specified stress	135 psi	125 psi	115 psi
area of the fillet (in^2)	132.612	133.824	134.326

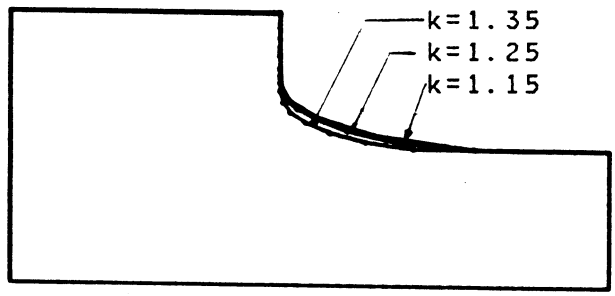

Figure 5-17 Optimum Shape for the 2-D Fillet

very smooth. In this example, the different optimum shapes can be obtained by specifying a different stress concentration factor. The total computer time required for the optimization process is about 63 minutes.

5.5.4 Optimal Shape Design of a Ladle Hook

This example concerns the design of a hook for lifting hot-metal ladles with a minimum weight of 150 tons. The dimension of the critical elements of the hook (Figure 5-18) on the basis of stress is presented by Dieter, 1983. These dimensions have been based on keeping the nominal stress at a level below 12,500 psi. The remaining dimensions such as the bight section are set by engineering common sense. In the example, the design objective is to minimize the cross-sectional area of the ladle hook in order to get the optimal bight section. Stress constraints are imposed which require the stress along the hole (curve EF) to be less than the nominal stress.

The problem is analyzed by the substructuring analysis method with the boundary element method. The ladle hook is divided into two substructures (Figure 5-19). Substructure 1 is discretized by 47 quadratic boundary elements. Substructure 2 is discretized by 46 quadratic boundary elements. The curve between points A and B is considered as a design patch which is created by 17 boundary elements (35 nodes). The design patch is generated by a 7th order

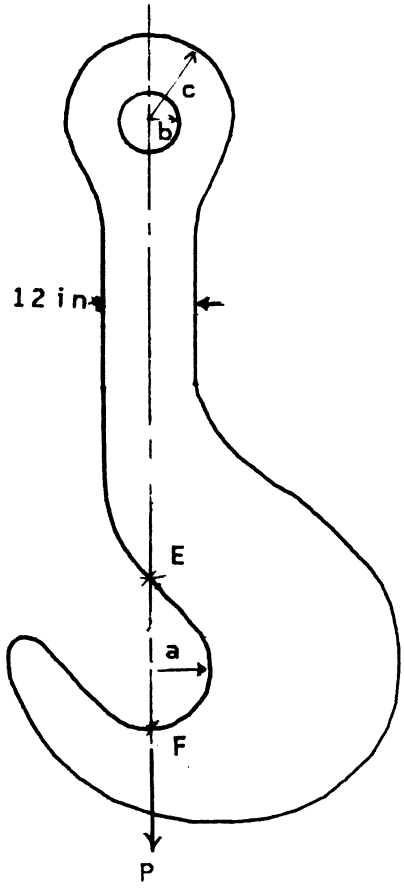

a=8 in
b=4 in
c=10.5 in
P=75 tons
thickness=7.1 in

Figure 5-18 The Dimensions and Loading for the Ladle Hook

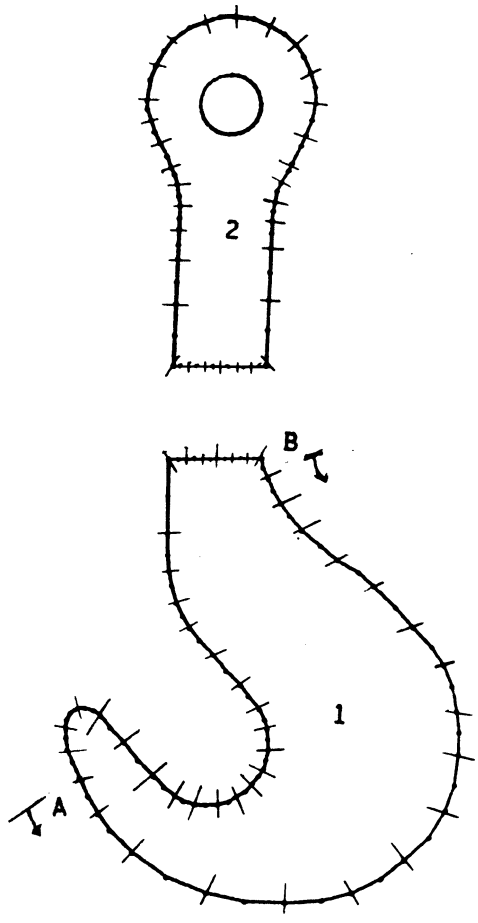

x is control point

Figure 5-19 The Boundary Element Mesh for the Ladle Hook

B-spline curve which has 9 control points. So there is a total of 18 design variables.

The formulation of the optimization problem is described as follows:

Minimize A

$$\text{Subject to } (\sigma_0 - (\sigma_j + \sum_{i=1}^{I} \frac{\partial \sigma_j}{\partial v_i} \delta v_i))/\sigma_0 \geq 0 \quad j=1,2...n \qquad (5\text{-}29)$$

and $c_i \geq v_i \geq d_i$

A is area of fillet

σ_0 is the specified stress (12,500 psi)

σ_j are stresses at the jth node of boundary elements on curve CD

v_i are the variations of the design variables

I is the total number of design variables.

c_i and d_i are the move limits on the design variables

n=17 is the total number of nodes on curve CD

The optimum shape of the bight section of the ladle hook is shown in Figure 5-20. The area of the bight section was reduced by 244.82 in^2. In this example, the coefficient matrix of substructure 2 was changed during every boundary element analysis because of the variation of the boundary. Combining the new coefficient matrix of substructure 2 with the fixed coefficient matrix of substructure 1 can produce a relatively small order system equation in terms of the interfaced boundary only. This substructuring analysis saved two-thirds of the computer time required for the whole analysis for every evaluation. The reason that the whole

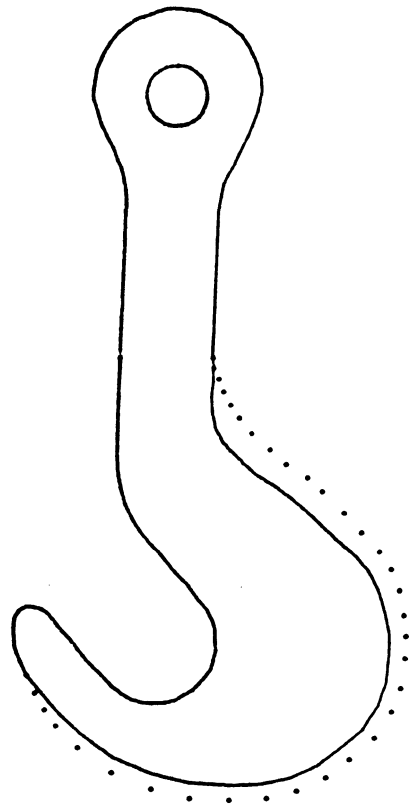

..... initial profile
——————— optimum profile

Figure 5-20 The Optimum Shape for the Ladle Hook

boundary element method wasn't used for the optimization was because the solutions generated were poor, even when the double precision version of the program was used.

The design process took 209 function analyses and 229 constraint evaluations. The total computer time for the optimization process was twelve hours and thirty minutes on a VAX 11-780. The final shape for the ladle hook was verified by the finite element method. The finite element mesh is shown in Figure 5-21. The problem was discretized using 53 quadratic quadrilateral 8-node elements with 211 nodes. The maximum stress computed for the problem was 12,380 psi which is lower than the nominal stress.

5.5.5 Optimum Tapering of a Cantilever Beam.

This example is concerned with finding the optimum tapering of a cantilever beam with a rectangular cross-section of given uniform width. The dimensions and loading for the beam are shown in Figure 5-22. This optimization problem with stress constraints imposed has a simple closed-form solution (Imam 1982). Based on the assumption of constant boundary stress, the minimum mass shape is given by

$$y=\sqrt{\frac{6Px}{b\sigma}} \qquad (5\text{-}30)$$

where

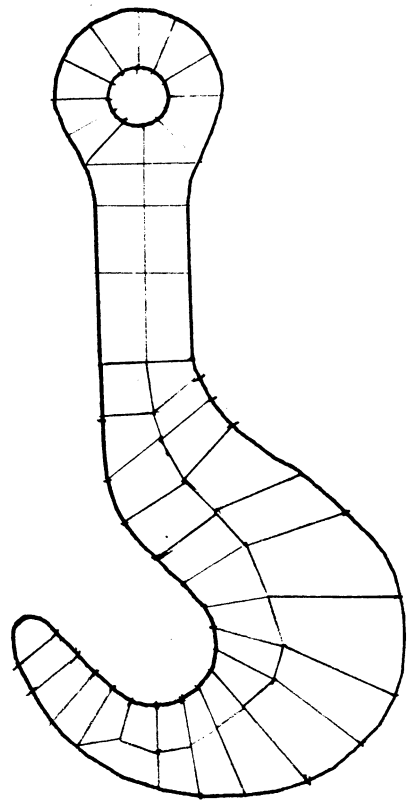

Figure 5-21 The Finite Element Mesh for the Ladle Hook

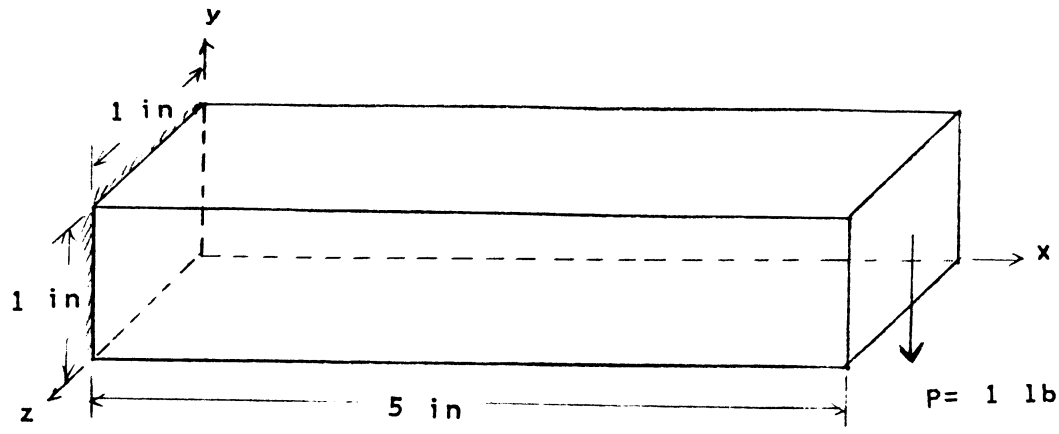

Figure 5-22 The Dimensions and Loading for the Cantilever Beam

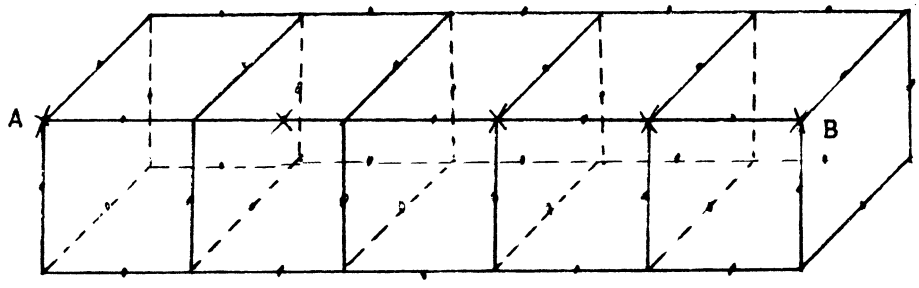

x is control point

Figure 5-23 The Boundary Element Mesh for the Beam

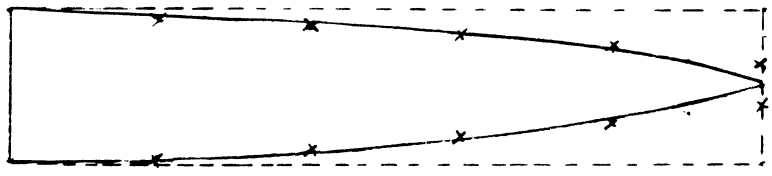

x x x numerical result

——— analytical result

Figure 5-24 The Optimum Tapering Shape for the Catilever Beam

y is the depth of the beam of any cross-section at a distance x from the free end of the beam.

b is the width of the beam.

σ is the value of the maximum allowable boundary stress. (σ=30 psi in this example)

P is the force acting at the free end. (p=1 lbf)

The boundary element model is shown in Figure 5-23. The three-dimensional beam is discretized by 22 quadratic quadrilateral 8-node elements. Using symmetry and constant width conditions, the shape of curve between points A and B is defined by a 4th order B-spline curve with 5 control points. Control points 2 through 5 are movable in the y-direction.

The optimum tapering for the beam is shown in Figure 5-24. The numerical results are in close agreement with the theoretical optimum shape. The difference in the shape at the end is due to geometry constraints which were imposed to avoiding distorting the elements.

5.5.6 Optimal Shape Design of a Three-dimensional Fillet.

This example is concerned with the optimum shape of the transition surface connecting two surfaces of different depths under an axially distributed constant loading (Figure 5-25). The design objective is to minimize the weight for the problem by generating an optimum shape for the fillet which has a maximum stress less than the allowable stress.

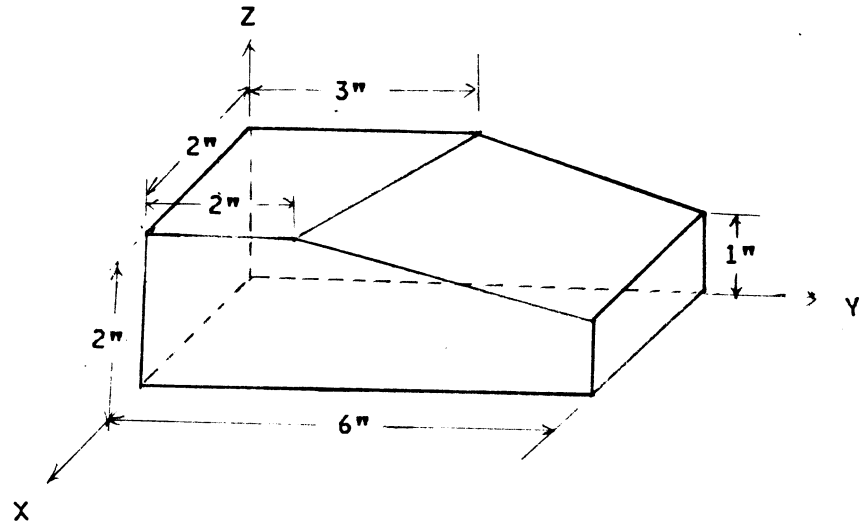

uniform y-axial loading:

p_1=100 lb/in^2 at y=2 in

p_2=-50 lb/in^2 at y=0 in

Figure 5-25 The Dimensions and Loading for the 3-D Fillet

The problem is modeled by 26 quadratic quadrilateral 8-node boundary elements (Figure 5-26). The surface ABCD is considered as a design patch which has 5 elements (28 nodes). The surface of the design patch is defined by 4 control points in the x-direction and 2 control points in the y-direction.

The formulation of the problem is similar to that of the two-dimensional fillet. The specified maximum allowable stress for the problem is 135 psi (i.e. the stress concentration factor is 1.35). Starting from an initially straight plane, the design process took 212 constraint evaluations and finally achieved the optimum shape (Figure 5-27). The minimum volume of the fillet is 17.63 in^3 out of 20.5 in^3.

5.6 Conclusion

In the examples discussed above, the order of the B-spline curves that define the design patch was selected to have the same order as the Bezier curves. The higher order B-splines provide a very smooth curve and/or surface for the design shape. A lower order for the B-splines could be used to represent the design shape, but the order should not be so low as to allow for an unrealistic design. The basic concern is that the independent movements of a control node

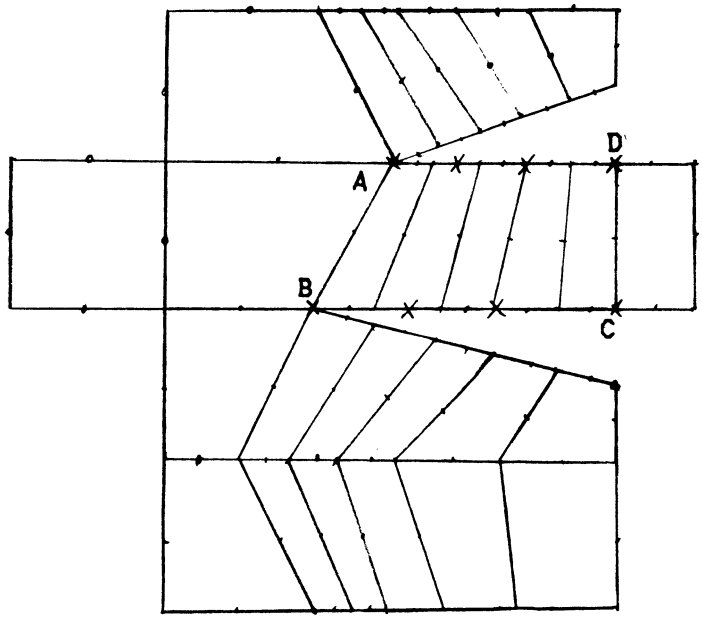

x is control point

Figure 5-26 The Boundary Element Mesh for the 3-D Fillet

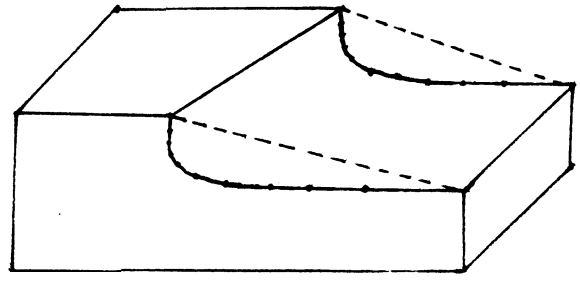

..... initial profile
——— optimum profile

Figure 5-27 The Optimum Shape for the 3-D Fillet

in the boundary element mesh would provid local control only which could allow the design shape to have a ripple.

The B-spline and Bezier techniques can be easily used to discretize the boundary element mesh by specifying the value of the influence parameter u. The boundary element mesh for the new shape is generated by line elements for the B-spline curve and by surface elements for the B-spline surface. They merge well together because no internal boundary element mesh is required.

In the shape design for the three-dimensional problem, the neighboring boundary should be carefully monitored in order to avoid distorted elements during the optimization. Such a problem with the three-dimensional boundary element mesh is still much easier to handle than the same problem using a three-dimensional finite element mesh. The possibility of distorted elements dosen't arise in the shape design of two-dimensional problems using the boundary element method.

In the examples presented, the design variables for the optimization problem are not necessarily the nodal points of the boundary element mesh. The design variables are defined by the moving direction of the control points. The distance between neighboring control points does not need to be equally spaced. The region defining a complex shape can be specified by more control points. In addition to the shape representation using B-splines, the parametrical representation of the shape optimization of structures such

as the radius of a circle, position or length of straight line segments,etc can also be considered as design variables in the optimization process.

The numerical results for the examples are satisfactory when compared with either exact results or finite element solutions, but there is one thing which is a cause for some concern. The computer time required for the optimization process is large. Even though the analysis of a single case is efficient, more than a hundred evaluations of the boundary element analysis requires a fairly large amount of computer time during the optimization process. This condition can be improved by formulating the problem using the substructuring analysis technique and also by calculating the gradients by Equation 5-10. In Equation 5-10, the gradient of the coefficient matrices are computed using the finite difference method which still takes considerable time during the formation of the matrices especially for a big problem. The possible ways to reduce computer time are to find the gradient of the problem by an analytical method instead of the finite difference method and also to minimize the number of boundary element analyses by using approximate methods such as a Taylor series expansion of the constraints. These methods have been applied to structural optimization using the finite element analysis.

CHAPTER 6

CONCLUSION

The boundary element programs have been developed using linear and isoparametric quadratic line elements for solving plane strain and plane stress problems and using linear and isoparametric quadratic quadrilateral surface elements for solving three-dimensional elasticity problems. Results for practical elasticity problems without body forces have been presented and the usage of different element types has been demonstrated. The boundary element solutions offer several advantages over the domain type solution procedures, such as the finite element method. These advantages include the possibility of defining only the surface of the body and the accuracy of the solutions are especially well suited to shape optimization.

The computer program for substructuring analysis by the boundary element method has been developed using isoparametric quadratic line and quadrilateral boundary elements. The results for practical problems of two- and three-dimensional elasticity have been successfully solved. The substructuring analysis by the boundary element method provides a versatile tool for the optimization process. The boundary element analysis for the unmodified substructure

only needs to be formulated once. The final system equation for the whole structure is assembled by the system equation for each substructure in terms of the interfaced displacements. The solution for the substructures generate the displacements and stresses on the interface. Additional solution information is calculated for each substructure independently. It is not necessary to calculate all the displacements and stresses on each substructure. Selected information is available for the objective function and/or the constraints needed during the optimization.

As seen from the numerical examples of structural shape optimization, the design objective of the optimization problem is to minimize either the weight or the peak stress of a structure, subject to geometrical and stress constraints. The B-spline and the Bezier techniques are introduced to describe the shape of the design. The control points on these curves are the design variables. The formulation of the boundary element method is accomplished through the use of quadratic line and quadrilateral elements. The numerical results for practical plain strain, plain stress and three-dimensional problems have been successfully generated by combining the boundary element program with the optimization code OPT. The major advantages of this optimization process are:

(1) The boundary element method provides very accurate boundary response, especially for the boundary stress.

(2) There is no need for an internal mesh in the boundary element model, so the element mesh is updated easily during the optimization process.

(3) The number of design variables can be reduced by applying B-spline or the Bezier techniques to represent the boundaries.

(4) The computer time is reduced by applying a substructuring analysis in conjunction with the boundary element method.

REFERENCES

Banerjee, P.K. and Butterfield, R. 1979, Developments in Boundary Element Methods. Vol. 1 APPLIED SCIENCE PUBLISHERS LTD.

Banerjee, P.K. and Butterfield, R. 1980, Boundary Element Methods in Engineering Science. McGRAW-HILL

Beer, F.P. and Johnston, E.R. 1981, Mechanics of Materials. McGRAW-HILL

Brebbia, C.A. 1978, The Boundary Element Method for Engineers. JOHN WILEY & SONS

Brebbia, C.A. 1978, Recent Advances in Boundary Element Methods PENTECH PRESS

Brebbia, C.A. 1981, Progress in Boundary Element Methods Vol 1 JOHN WILEY & SONS

Brebbia, C.A. 1981, Boundary Element Methods. Proceedings of the Third International Seminar, Irvine, California. (Editor Brebbia, C.A.) CML Publications

Brebbia, C.A. 1982, Boundary Element Methods. Proceedings of the Fourth International Seminar, Irvine, California. (Editor Brebbia, C.A.) CML Publications

Brebbia, C.A. 1984 , Boundary Element Techniques in Computer-Aided Engineering. MARTINUS NIJHOFF PUBLISHERS.

Braibant, V. and Fleury, C. 1984, "Shape Optimal Design Using B-splines." Computer Methods in Applied Mechanics and Engineering Vol 44, pp 247-267

Chun, Y.W. and Haug, E.J. 1978, "Two-Dimensional Shape Optimal design." International Journal of Numerical Methods in Engineering Vol 13, pp 311-336

Dems, K. and Mroz, Z. 1978, "Multiparameter Structural Shape Optimization by the Finite Element Method." International Journal of Numerical Methods in Engineering vol 13, pp 247-263

Dieter, G.E. 1983, Engineering Design : A Materials and Processing Approach McGRAW-HILL

Gabriele, G.A. and Ragsdell, K.M. 1976, OPT: A Nonlinear Programing Code in FORTRAN IV Users Mannual. Purdue Research Foundation. West Lafayette, IN.

GTSTRUDL User's Manual, 1983, Georgia Tech STRUDL User's Manual Georgia Institute of Technology Atlanta, Georgia

Imam, M.H. 1982, "Three-dimensional Shape Optimization." International Journal of Numerical Methods in Engineering Vol 18, pp 661-673

Jaswon, M.A. Symn, G.T. 1978, Integral Equation Methods in Potential Theory and Elastostatics. ACADEMIC PRESS

Kristensen, E.S. and Madsen, N.F. 1976, "On the Optimization Shape of Fillets in Plates Subjected to Multiple In-Plane Loading Cases." Int. J. Num. Meth in Engng, Vol 10 , pp. 1007-1019

Kunar, R.R. and Chan, A.S.L. 1976, " A Method for the Configurational Optimization of Structures." Computer Methods in Applied Mechanics and Engineering Vol 7, pp 331-350

Lachat, J.C. and Watson, J.O. 1976, "Effective Numerical Treatment of Boundary Integral Equations: A Formulation for Three-dimensional Elastostatics." International Journal of Numerical Methods in Engineering
Vol. 10 pp 991-1005

Mota Soares, C.A. , Rodrigues, H.C. , Oliveira Faria, L.M. and Haug, E.J. 1983, "Optimization of the Geometry of Shafts Using Boundary Elements." ASME 83-DET-34

Mota Soares, C.A. , Rodrigues, H.C. , Choi, K.K 1984, "Shape Optimal Structural Design Using Boundary elements and Minimum Compliance Techniques." ASME 84-DET-57

Newman, W.M. and Sproull, R.F. 1979, Principles of Interactive Computer Graphics. McGRAW-HILL

Ovadia, E.L. 1981, Structural Optimization Recent Developments and Applications. (Edited by Ovadia, E.L.) ASCE

Przemieniecki, J.S. 1968, Theory of Matrix Structural Analysis. McGRAW-HILL

Reklaitis, G.V. , Ravindran, A. and Ragsdell, K.M. 1983, Engineering Optimization Methods and Applications. JOHN WILEY & SONS

Rosen, R. and Rubinstein, M.F. 1970, "Substructure Analysis by Matrix Decomposition." Journal of the Structural Division, Proceeding of the ASCE pp 663-670

Schnack, E. 1979, "An Optimization Procedure for Stress Concentrations by the Finite Element Technique." International Journal of Numerical Methods in Engineering Vol 14 pp. 115-124

Stroud, A.H. and Secrest, D. 1966, Gaussian Quadrature Formulas Prentice Hall, Int. Inc. London

Timoshenko, S.P. and Goodier, J.N. 1970, Theory of Elasticity. Third Edition, McGRAW- HILL

Tvergaard, V. 1975, "On the Optimum Shape of a Fillet in a Flat Bar with Restrictions." Optimization in Structural Design (Ed. Sawczuk, A. and Mroz, Z.) Springer-Verlag New York, pp. 181-195

Zienkiewicz, O.C. and Campbell, J.S. 1973, "Shape Optimization and Sequential Linear Programing." Optimum Structural Design (editor R.H. Gallagher and O.C. Zienkiewicz) Wiley, New York, PP. 109-126

VITA

Shyue-Jian Wu was born [redacted], in Taiwan, R.O.C.. He was graduated from Shinchu High School, Shinchu, Taiwan, R.O.C. in 1972. He received both his B.S. (1977) and M.S. (1981) in Mechanical Engineering from the National Cheng Kung University, Tainan, Taiwan, R.O.C. and his Ph.D. (1986) in Mechanical and Aerospace Engineering from the University of Missouri-Columbia, Columbia, Missouri. He is married to Ye-Ling, and they have a lovely boy, Shipher.

University Libraries
University of Missouri

Digitization Information Page

Local identifier Wu1986

Source information

Format	Book
Content type	Text
Source ID	Gift copy from department; not added to MU collection.
Notes	

Capture information

Date captured	March 2024
Scanner manufacturer	Fujitsu
Scanner model	fi-7460
Scanning system software	ScandAll Pro v. 2.1.5 Premium
Optical resolution	600 dpi
Color settings	8 bit grayscale
File types	tiff
Notes	

Derivatives - Access copy

Compression	Tiff: LZW compression
Editing software	Adobe Photoshop
Resolution	600 dpi
Color	grayscale
File types	pdf created from tiffs
Notes	Images cropped, straightened, brightened